Cell Reports

Article

Social remapping of spatial coding along the dorsoventral axis of the mouse prefrontal cortex

Graphical abstract

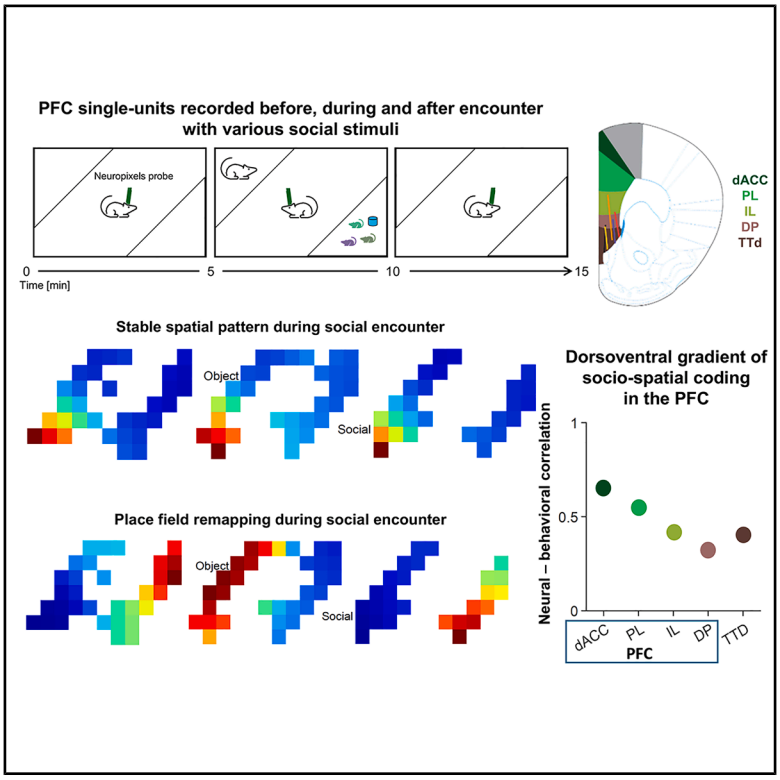

Highlights

- Mouse behavior and single PFC unit activity exhibit socio-spatial tuning
- Behavioral and neuronal socio-spatial tuning are correlated
- In the presence of social stimuli, PFC single-units undergo remapping of their spatial coding
- Socio-spatial modulations exhibit dorsoventral gradients within the PFC

Authors

Lear Cohen, Alok Nath Mohapatra, Shai Netser, Shlomo Wagner, Eran Stark

Correspondence

learcohen1510@gmail.com (L.C.), shlomow@research.haifa.ac.il (S.W.), eranstark@sci.haifa.ac.il (E.S.)

In brief

Cohen et al. reveal the functional organization of the mouse prefrontal cortex that enables gradual modulation of neuronal spatial representation by social context. This organization follows a dorsoventral gradient, dictated by topologically organized groups of neurons showing differential encoding of spatial and social aspects of the individual's behavior.

Cohen et al., 2025, Cell Reports *44*, 116319
October 28, 2025
https://doi.org/10.1016/j.celrep.2025.116319

CellPress

Cell Reports

CellPress
OPEN ACCESS

Article

Social remapping of spatial coding along the dorsoventral axis of the mouse prefrontal cortex

Lear Cohen,[1,5,6,*] Alok Nath Mohapatra,[2,3,4,5] Shai Netser,[1] Shlomo Wagner,[1,*] and Eran Stark[1,*]
[1]Sagol Department of Neurobiology, Faculty of Natural Sciences, University of Haifa, Haifa, Israel
[2]Department of Psychiatry, Massachusetts General Hospital, Harvard Medical School, Boston, MA, USA
[3]Harvard Stem Cell Institute, Cambridge, MA, USA
[4]Broad Institute of MIT and Harvard, Cambridge, MA, USA
[5]These authors contributed equally
[6]Lead contact
*Correspondence: learcohen1510@gmail.com (L.C.), shlomow@research.haifa.ac.il (S.W.), eranstark@sci.haifa.ac.il (E.S.)
https://doi.org/10.1016/j.celrep.2025.116319

SUMMARY

Neuronal representation of space remaps between spatial contexts, but little is known about spatial modulation across social contexts. We analyze extracellular recordings from single neurons in the prefrontal cortex (PFC) of adult male mice freely exploring an arena during four distinct social contexts. Neuronal spatial preferences vary across social contexts and differ between PFC subregions. By comparing the spatial and social aspects of behavior and their neuronal correlates, we find that correlations between behavioral and neuronal representations decrease monotonically along the PFC dorsoventral axis. Some single-unit groups show place remapping and modulation of activity in the presence of social stimuli. The prevalence of spatially tuned units decreases dorsoventrally, while the prevalence of socially tuned units increases along the same axis. Thus, social context dynamically modulates spatial representations in mouse PFC, revealing a topologically organized trade-off between spatial and social encoding along the dorsoventral axis.

INTRODUCTION

Understanding space encoding by neuronal activity is fundamental to grasping the complex cognitive processes behind spatial navigation and memory. Neuronal representations of space were studied in multiple animal models,[1–4] where cognitive maps were characterized.[5] Spatial representations were highly dynamic—neuronal place fields and spatial maps are modulated or remapped, following environmental changes over time[6,7] and contexts.[8]

Social factors play a crucial role in spatial navigation,[9] allowing an individual to avoid rivals, find group members, or locate a mate. This requires integrating social and spatial representations in the same neuronal infrastructure to create a socio-spatial cognitive map.[10] For example, single neurons in the hippocampal CA1 region encode the position of conspecifics in both allocentric and egocentric coordination systems.[11–13] Such integration is vital for territorial behavior, which is common among mammals, including humans.[14] Nevertheless, where and how the representations of physical space and social environment are integrated in the brain is not fully understood.

We hypothesize that insights into brain integration of spatial and social representations may be gained by studying the prefrontal cortex (PFC). From the spatial aspect, the murine PFC is involved in goal-directed behavior,[15] trajectory planning,[16] and rule switching.[17] From the social aspect, the PFC is implicated in social behavior[18,19] and decision-making,[20] and single PFC units fire in proximity to conspecifics.[21] Moreover, studies from our lab show that different social contexts mediate behavior and neural activity in the PFC[22,23] and that pyramidal cells in mouse PFC discriminate affective states.[24] Thus, PFC neurons appear to be involved in social and spatial representations, making the PFC a suitable candidate for integrating social and spatial information into a socio-spatial cognitive map. Accordingly, neurons in the prelimbic (PL) area of the PFC encode a combination of social and spatial information during a social task.[25] However, it remains unknown how this socio-spatial coding is modulated in different social contexts and whether it has a subregion-specific organization in the PFC.

Here, we investigate the neuronal representations of space and social context by single-unit spiking activity along the dorsoventral axis of the adult male mouse PFC. Each subject was tested during four distinct social contexts. Concurrently, PFC extracellular activity was recorded using a Neuropixels probe[24] implanted through the following cortices (dorsal to ventral): the anterior cingulate (ACC), PL, infralimbic (IL), dorsal peduncular (DP), and dorsal taenia tecta (TTd). The social and spatial aspects of neuronal activity were assessed across the different contexts and subregions to characterize the conjunction of social stimuli and spatial representation in the mouse PFC.

RESULTS

The paper is organized as follows. First, we describe the process of single-unit recordings during different social contexts

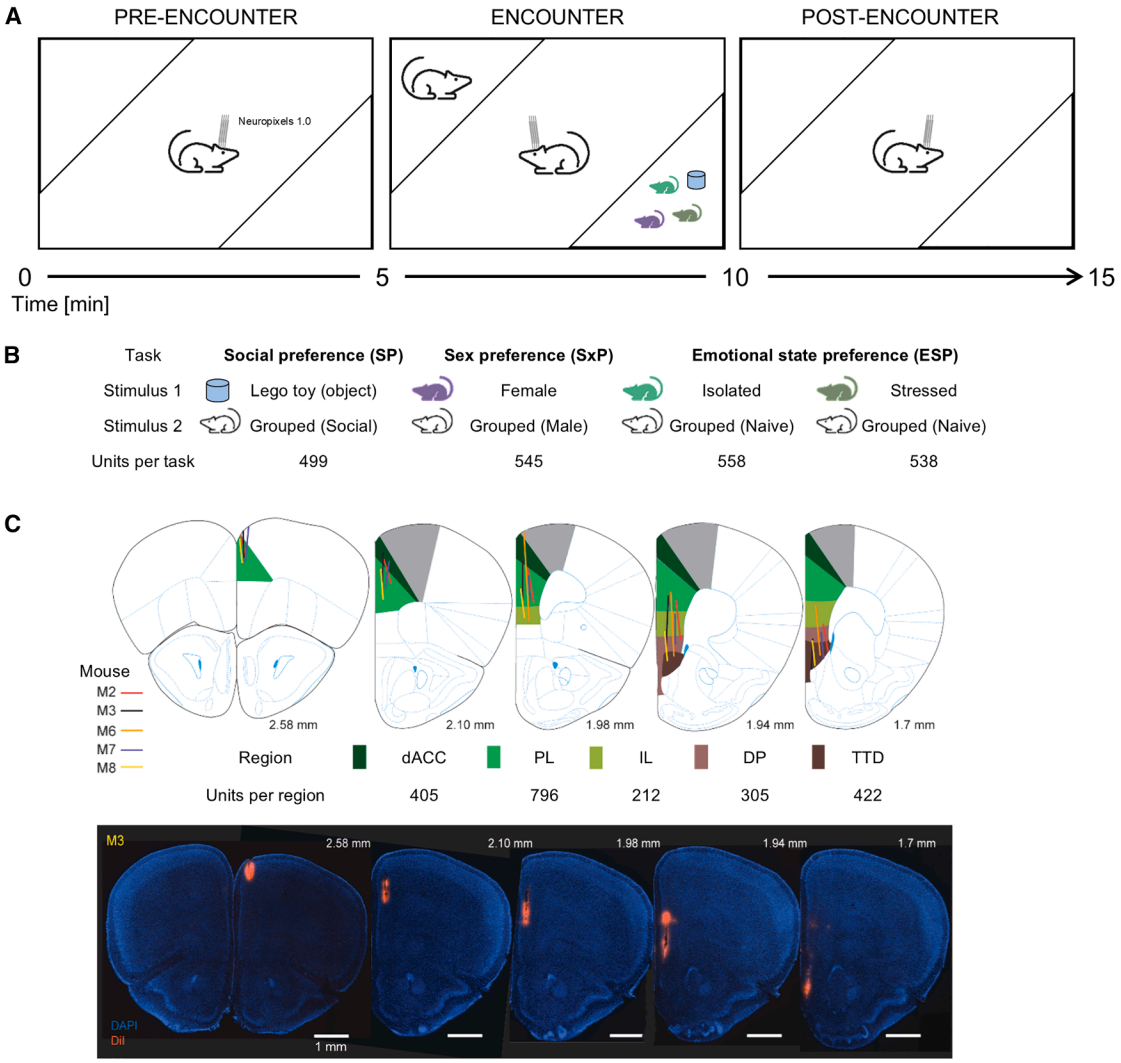

Figure 1. A dataset of 2,140 well-isolated single units was recorded from the PFC of five mice during four social contexts

(A) Schematics and timeline of a single recording session. Stimulus chambers (right-angled isosceles) are placed in opposite corners of the arena. The recorded mouse, chronically implanted with a Neuropixels 1.0 probe, freely explores the central part of the arena during three consecutive 5-min epochs. Social stimuli occupy the chambers only during the middle "encounter" epoch.

(B) Tasks and corresponding stimuli. Icons correspond to icons in A.

(C) Top: probe tracks through the PFC for all mice. Middle: number of units recorded from every subregion. dACC, dorsal anterior cingulate cortex; PL, prelimbic cortex; IL, infralimbic cortex; DP, dorsal peduncular cortex; and TTd, dorsal taenia tecta. Bottom: coronal brain slices from mouse M3, with probe track labeled with DiI. Scale bars, 1 mm.

(Figures 1 and S1). Then, we assess the relationship between social and spatial aspects of behavior vs. neural representations among the recorded units (Figures 2 and S2). Then, we assess spatial preferences before and during the presence of different social stimuli at the population level (Figure 3). Next, we identify four mutually exclusive groups of units (Figures 4, 5, S4, and S5), each of which exhibits a distinct modulation of firing patterns during the presence of social stimuli. Finally, we focus again on the population level and estimate the prevalence of social vs. spatial effects across social contexts and PFC subregions (Figures 6 and S6).

Recording PFC neuronal activity in four distinct social contexts

To examine whether neuronal encoding of space in the PFC varies during social interactions in distinct contexts, we chronically implanted Neuropixels 1.0 probes in the PFC of five adult male CD1 mice.[24] Each mouse was tested during four social tasks, each of a different context (using a distinct pair of stimuli). One stimulus ("stimulus 1"; Figure 1B) differed between tasks: an inanimate object (a Lego toy) in the social preference (SP) task; a female mouse in the sex preference (SxP) task; a 1-week socially isolated male mouse in the isolation

A

	Behavior	PL unit	TTd unit
	Time [s]	Rate [spikes/s]	Rate [spikes/s]
Pre-encounter	T1=53 T2=79	R1=15.4 R2=4.3	R1=1.5 R2=1
Encounter	T1'=155 T2'=112	R1'=11.7 R2'=4	R1'=2.5 R2'=3.6
Dkl spatial	0.02	0.22	0.001
Dkl social	0.1	0.01	0.23
	BCI = -0.62	**NCI = 0.95**	**NCI = -0.99**

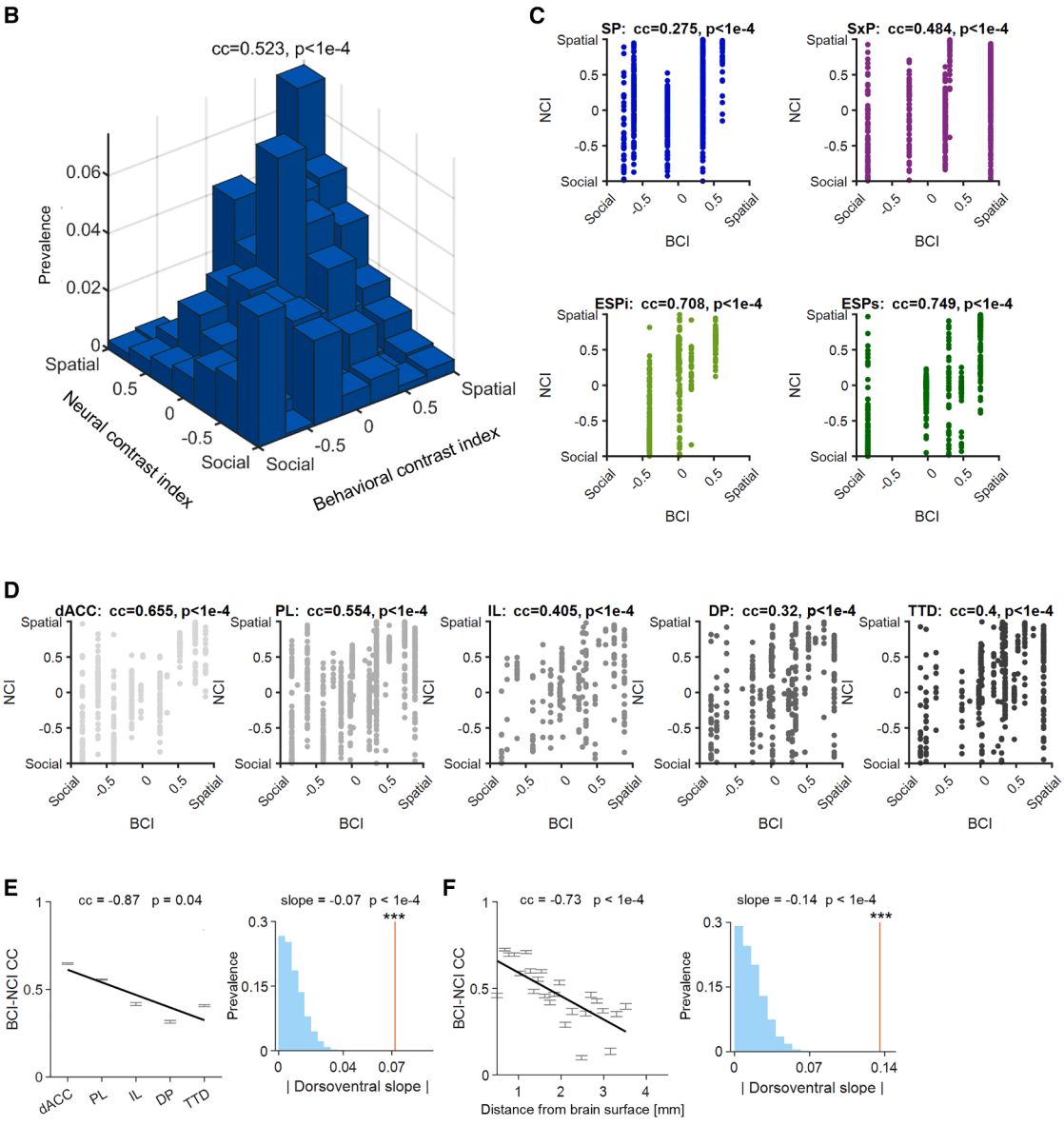

Figure 2. Correlation between behavioral and neuronal preferences in socio-spatial space decreases dorsoventrally along the PFC

(A–D) Neuronal contrast index (NCI) vs. behavioral contrast index (BCI). (A) Example session BCI and NCI of two simultaneously recorded units (mouse M2, ESPi task). For each unit, the chamber investigation durations during every epoch and the corresponding firing rates near each chamber are indicated. Spatial and social Kullback-Leibler divergences (D_{KL}) and the derived BCI and NCI values are also indicated. (B) Joint probability histogram of the NCI vs. BCI ($N = 2140$ units). Bin size, 0.285 × 0.285. (C) BCI-NCI scatter per task. Each panel includes behaviors from five different mice. In every panel here and in (D), text indicates the rank (Spearman's) correlation coefficient (cc) and the corresponding p value. (D) BCI-NCI scatter per PFC subregion. Each panel includes 20 different values, corresponding to five mice × four tasks.

(legend continued on next page)

emotional-state preference (ESPi) task; and a stressed (restrained before the task) male mouse in the stress emotional-state preference (ESPs) task.[24] The reference stimulus (“stimulus 2”) was similar in all tasks: a naive group-housed male mouse. Animal movement and extracellular electrophysiological signals were simultaneously recorded while the mice freely explored two triangular stimulus chambers located at opposite corners of the rectangular experimental arena during a 15-min session. Each session was divided into three consecutive 5-min epochs (Figure 1A): pre-encounter, encounter, and post-encounter. During the pre- and post-encounter epochs, the stimulus chambers were empty. During the encounter epoch, each stimulus was randomly located in one of the two chambers (Figure 1A, middle panel).

During the 20 sessions (four tasks in $N = 5$ mice), 4,189 candidate units from the five PFC subregions (Figure 1C) were automatically isolated by Kilosort. We determined the isolation quality of the units (Figure S1) using a combination of a temporal isolation metric (inter-spike-interval (ISI) index[26] below 0.2) and a waveform isolation metric (L-ratio[27]). A dataset of 2,140 well-isolated single units passed our quality check (Figure S1D) and comprised a median of 440 units per mouse (range, [104, 833]). The median ISI-index was 0.02 (interquartile range, IQR [0, 0.11], $N = 2140$ units) and the median [IQR] L-ratio was 0.001 [0.0001, 0.01]. Over $N = 20$ sessions, the number of spikes collected was 2,087 [1,023, 5,171]. Among the 2,140 single units, the largest subset (796 units) was from the PL (Figure 1C; Table S1).

Behavioral and neuronal preferences in the socio-spatial space are correlated

To test whether socio-spatial representations by neuronal spiking activity are associated with behavioral preferences, we first quantified the social and spatial derivatives of mouse behavior during the different tasks. We calculated the investigation durations, namely the times the animal was approaching each stimulus chamber, during the pre-encounter (T1 and T2; Figure S2A) and encounter (T1′ and T2′) epochs, extracting a set of four numbers (animal-specific values are shown in Figure S2A). We then estimated how “socially-oriented” and how “spatially-oriented” the behavior of each mouse was in every session (toy examples of socially oriented and spatially oriented behaviors; Figure S2A, top right). This was done by comparing the observed proportions of durations with those expected under the null hypothesis of no social or spatial preference (a uniform prior; examples in Figure 2A). The analysis yielded two values of the Kullback-Liebler divergence (DKL), from which a behavioral contrast index (BCI) was derived (Figure 2A, left). The BCI is a scalar ranging from −1 for purely socially oriented behavior to 1 for spatially oriented behavior. Over the 20 sessions, the median DKL_social was 0.1 (IQR: [0.03, 0.17]), the DKL_spatial was 0.17 [0.07, 0.45], and the BCI was 0.02 [−0.26, 0.52]. These results suggest that social and spatial features influence mouse behavior similarly.

Second, a neuronal contrast index (NCI) was calculated for every unit to estimate how socially oriented and spatially oriented the neuronal activity of each unit was (examples in Figure S2A, bottom right). Here, we compared the number of spikes emitted by every unit with the null distribution given by the actual investigation durations during the pre-encounter (S1 and S2, Figure S2A) and encounter (T1′ and T2′) epochs. The NCI values range from −1 to 1 for purely socially to purely spatially oriented neuronal activity. Over the 2,140 units, the median [IQR] neuronal DKL_social was 0.14 [0.06, 0.3], the neuronal DKL_spatial was 0.2 [0.08, 0.43], and the NCI was −0.07 [−0.52, 0.38]. The examples of two units recorded simultaneously from different PFC subregions during the same ESPi session (i.e., with the same BCI) are shown in Figure 2A. The behaviorally preferred chamber changed when the social stimuli were introduced (pre-encounter, T1 > T2; encounter, T1’ < T2′). Thus, the behavior was more socially than spatially oriented, yielding a BCI of −0.62. However, the firing rates of the two units, i.e., the spike counts divided by the investigation durations, did not follow the same patterns. The PL unit exhibited a higher rate in proximity to the chamber of stimulus 1 during the pre-encounter (R1 > R2) and encounter (R1’ > R2′) epochs, yielding a spatially oriented NCI (0.95). In contrast, in the TTd unit, the higher firing rate shifted from stimulus 1 during the pre-encounter epoch to stimulus 2 during the encounter epoch (R1 > R2 and R1’ < R2′), yielding a social NCI (−0.99). This demonstrates that unit firing preferences do not necessarily follow animal behavior.

Despite the diversity of representations at the single-unit level, over the entire cohort of 2,140 units, the BCI values and the NCI values were correlated (Spearman’s rank correlation coefficient (cc), 0.523; $p < 0.001$, permutation test; Figure 2B). Comparing the BCI values with the NCI values for the subsets of data corresponding to different tasks, we found a significant correlation ($p < 0.001$) in all four cases (Figure 2C).

When we assessed the BCI-NCI correlation for the subsets of units recorded from the various PFC subregions, we found a significant correlation ($p < 0.001$) in all cases (Figure 2D). However, the correlation decreased monotonically along the dorsoventral axis (excluding the TTd; Figure 2E, left panel). Specifically, the BCI-NCI rank correlation was highest for the dACC units (0.66) and lowest for the DP units (0.32). This yielded a negative slope (−0.07) between the BCI-NCI rank correlations and the ordered subregions. A negative slope was observed for every animal (range: [−-0.15, −0.03]). The probability of obtaining the observed (or more) negative slope of correlation values along PFC subregions by chance was low ($p < 0.0001$, permutation test; Figure 2E, right panel). We also tested whether the inter-subregion correlation gradient is sensitive to the precise anatomical boundaries between PFC subregions. This was done by analyzing the slope of BCI-NCI correlations when units were grouped according to their distance from the brain surface (Figure 2F, left panel; each bin includes 89–90 units). We found

(E) Left: BCI-NCI correlation across subregions fitted with a line. Right: red line, observed absolute dorsoventral slope of the linear fit in the left panel. Cyan histogram, absolute slopes achieved by chance. Bin size, 0.004.
(F) Same as E, but with the depth of each unit from the brain surface. Bin sizes: left: bin size (mean ± SD), 0.14 ± 0.05 mm; right: 0.007. *** $p < 0.0001$, ISI shuffling test.

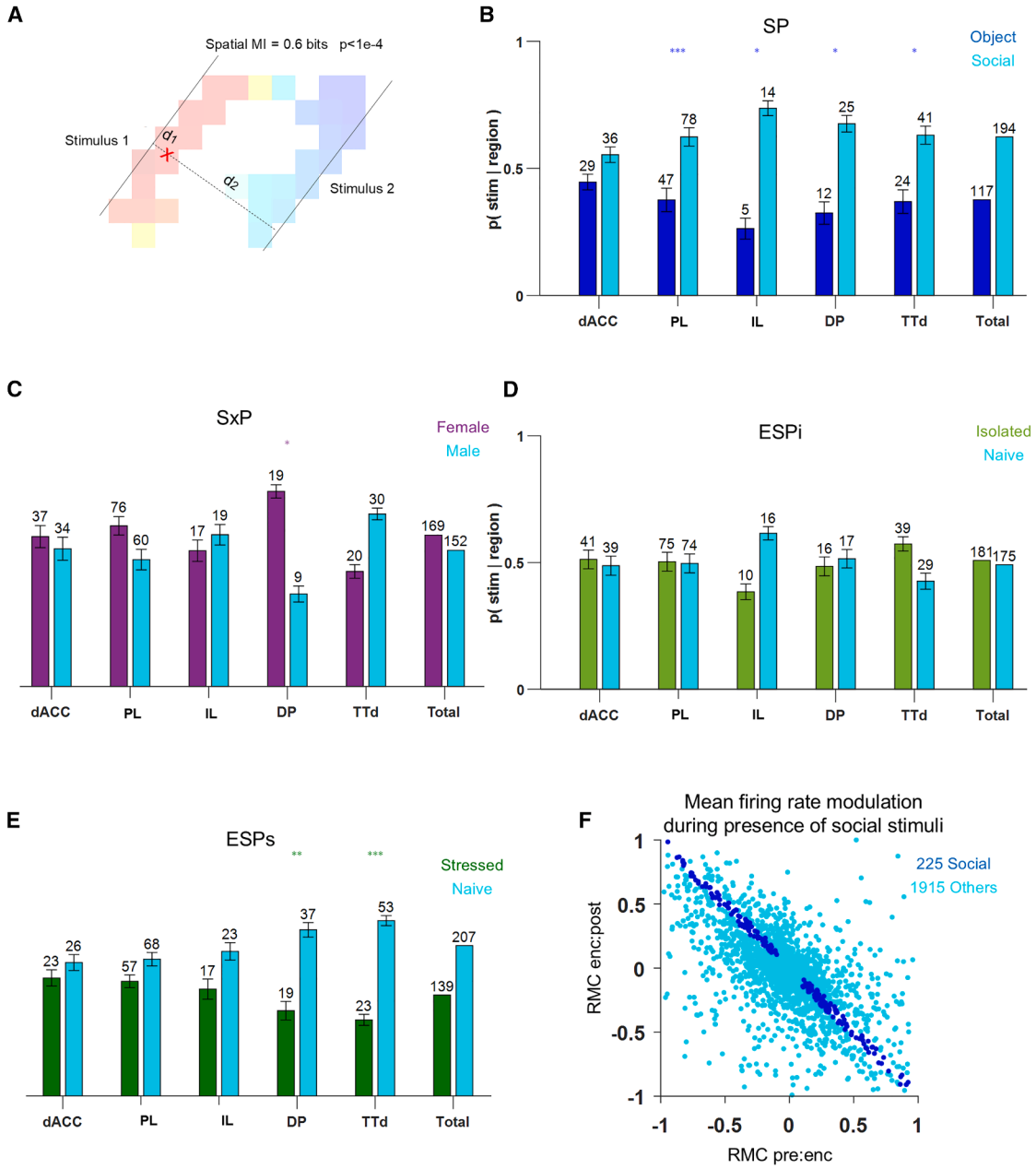

Figure 3. Neuronal spatial preferences vary across tasks and subregions

(A) Method used for classifying neuronal spatial preference, demonstrated using the same rate map as in Figure 4B. Red "X" marks the center of mass of the place field, i.e., the center of a unimodal Gaussian fitted to the neuronal firing rate map in space. Compared with the stimulus 2 chamber, stimulus 1 chamber is closer to the place field center (d1 < d2, dashed lines). Solid lines indicate chamber walls. This example unit exhibits a neuronal spatial preference to stimulus 1.

(B–E) Distributions of spatially modulated units according to the nearest stimulus chamber across the various PFC subregions during the SP, SxP, ESPi, and ESPs tasks. The number above each bar: single units exhibit a preference for the relevant stimulus in every subregion and task. Error bars, binomial errors. The proportions of each pair of preferences were tested for the null hypothesis of originating from the same distribution. **/***$p < 0.001/0.0001$, chi-squared test. Rightmost pair of bars: total preferences per task.

(F) Rate modulation contrast (RMC) for pre-encounter vs. encounter epochs and encounter vs. post-encounter epochs. Blue dots: 225 units that modulated their mean firing rate only when presented with social stimuli; cyan dots: 1,915 units that did not.

that the slope was negative and was steeper than can be achieved by chance ($p < 0.001$, permutation test; Figure 2F, right panel). These results suggest that both social and spatial aspects of the environment are represented in the PFC and demonstrate a dorsoventral gradient of socio-spatial neuronal encoding along the PFC dorsoventral axis.

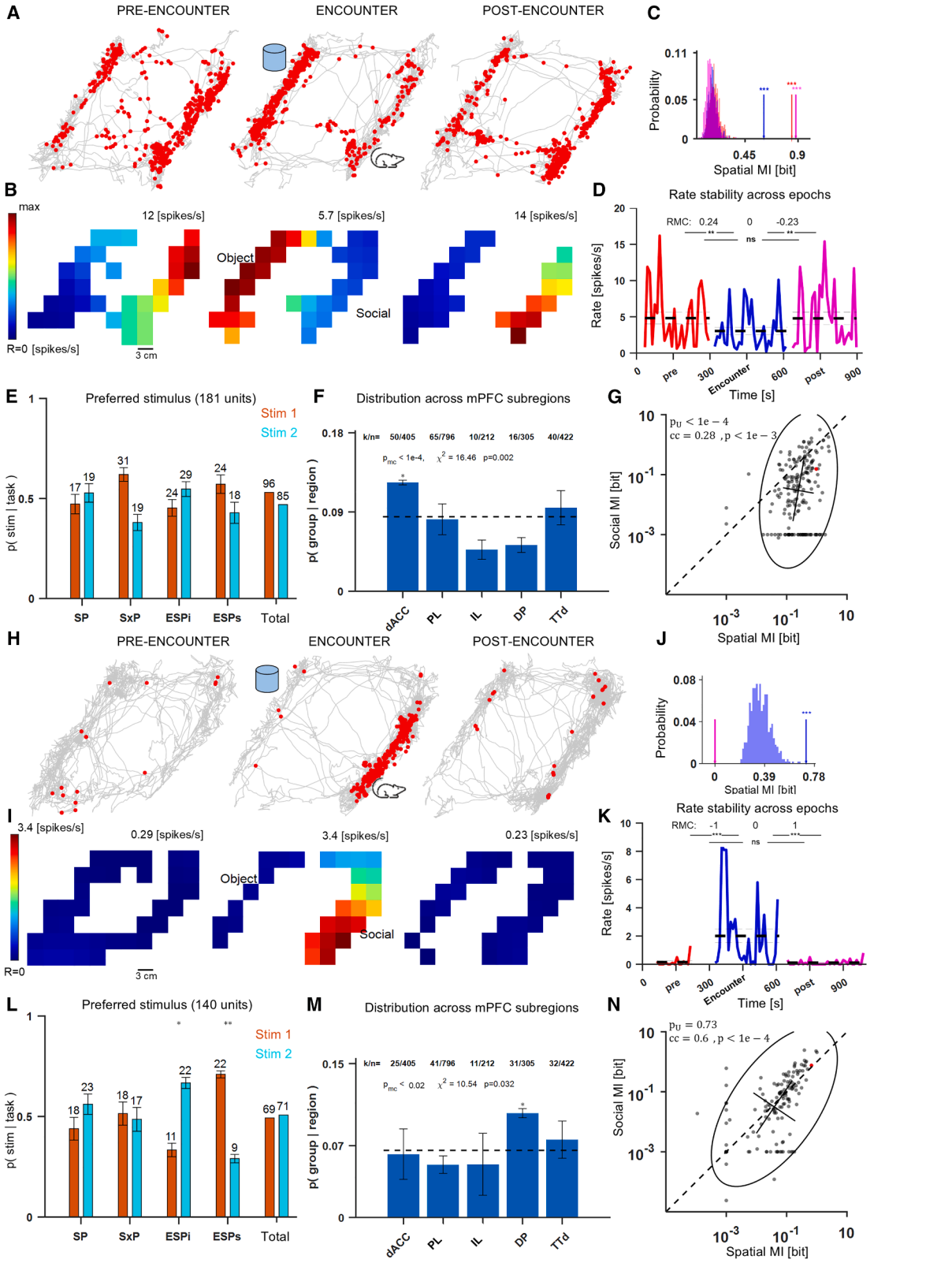

(legend on next page)

Neuronal spatial preferences during social encounters differ between tasks and PFC subregions

To test whether spatial preferences are uniformly represented in the PFC when social stimuli are present, we estimated the spatial preference of every unit, specifically during the encounter epoch. This was done by comparing the mutual information (MI) between mouse position in space and the spike train of every unit, with shuffled MI values obtained by shuffling the ISIs of the same spike train 5,000 times. To overcome dependency on entropy when comparing MI values, all MI-based analyses were de-biased by subtracting from each MI value the mean of the shuffled MI set generated from the same spike train. We employed a conservative criterion of $p < 0.05/3$ as "spatially informative" to allow a similar process in the other epochs. 1,334/2,140 (62%) units were spatially informative ($p < 0.0001$, binomial test compared to a chance level of 5%). Next, each of the 1,334 spatially informative units was associated with a stimulus chamber based on the distance between the center of the mass of the place field and the nearest neighboring stimulus chamber (example in Figure 3A). The distribution of these neuronal spatial preferences according to stimulus proximity along the different PFC subregions is shown for each task (Figures 3B–3E). During the SP task, more units preferred the side of the social stimulus over the Lego toy, yielding non-uniform distributions in most PFC subregions ($p < 0.0001$ for PL, $p < 0.01$ for the DP; and TTd; chi-squared test; Figure 3B). During the SxP task, only DP units showed a preference for the female over the male side ($p = 0.007$; Figure 3C). Distinct distributions were also observed for the two flavors of the ESP paradigm. During the ESPi flavor, no laterality bias was found in any of the subregions (Figure 3D). However, during the ESP flavor, a gradual non-uniform pattern emerged (Figure 3E): the proportion of units with preference to the side of the naive stimulus increased dorsoventrally and peaked at the DP ($p < 0.001$) and TTd ($p < 0.0001$). Notably, stressed and isolated stimuli were previously shown to elicit different neuronal responses in the PL,[24] as found here. Overall, the very different distributions of spatial preferences among the various tasks imply a social context sensitivity of spatial representation in the PFC.

Firing patterns modulated by the presence of social stimuli in the arena at the single-cell level

To quantify how single-unit spiking activity changes between two different epochs in a given session (e.g., from pre-encounter to encounter), we defined a rate modulation contrast (RMC). For every pair of epochs, the RMC was calculated as the difference between the mean rates of each epoch divided by their sum. The RMC values were then compared to chance, i.e., to RMC values obtained after ISI-shuffling. In 225/2,140 (10.5%) of the units (Figure 3F, blue dots), the mean epoch-resolved firing rate depended on the presence of social stimuli. Specifically, the firing rate was modulated after the pre-encounter epoch with the presence of social stimuli during the encounter epoch and returned to its initial value during the post-encounter epoch; it is manifested by RMC values for the pre-encounter vs. encounter and the encounter vs. post-encounter epochs, which are similar in absolute value but have opposite signs.

Together, the observations indicate that the spiking activity of individual units is modulated by the appearance of social stimuli during the encounter epoch (Figure 3F) and by the identity of those stimuli (Figures 3B–3E). This suggests an interaction between social and spatial preferences for units in mouse PFC. Therefore, we directly characterized the social and spatial components for each of the units and classified them into mutually exclusive sub-groups, each showing a unique socio-spatial pattern of neuronal activity. To discuss the sub-groups, we use the following terminology. "Social-place-remapping" describes units that change their spatial firing pattern when the only change in the environment is the presence of social stimuli (Figures 4A–4G), resembling the global remapping phenomenon observed in the hippocampus.[28] "Social-place-coding" refers to units that exhibit a clear spatial firing pattern only during the presence of social stimuli (Figures 4H–4N). "Social-rate-modulation" describes units with no apparent spatial firing pattern, which modulate their firing rate in the presence of social stimuli (Figures 5A–5F). The fourth group, units with a "stable-spatial-pattern" (Figures 5G–5M), includes units exhibiting similar spatial firing patterns with or without social stimuli in the arena, and the social effect on the activity of this group is assessed.

Place remapping of PFC units is induced by social stimuli

For each single unit, we quantified the spatial MI (as in Figure 3A) for each of the three epochs separately. In one example unit (spike waveforms and auto-correlation histogram (ACH) in Figure S3A), the spatial positions of the mouse when every spike occurred are presented over the trajectories during the three epochs (Figure 4A). This unit fired more spikes near the right

Figure 4. Place remapping and place coding of PFC units are induced during the presence of social stimuli

(A–D) An example of a social-place-remapping unit recorded from the PL during an SP task. See Figure S3A for spike waveforms and ACH. (A) Spikes (red dots) superimposed on trajectories (gray lines) taken by this mouse during the three epochs. (B) Rate maps: derived from the ratio between the spike count and the occupancy time in every bin. Colors code the firing rate, from zero (dark blue) to the maximum during each epoch (dark red, indicated above each panel). (C) Spatial MI during the pre-encounter (red), encounter (blue), and post-encounter (pink) epochs. Color-matched histograms (bin size, 0.01 bit) show the corresponding MI values derived from ISI-shuffled spike trains. (D) Rate over time during the three epochs (bin size, 10 s). Dashed thick and thin lines correspond to mean ± SEM over bins. Top: comparison of mean rates between epochs; ns/$^{**}p > 0.05/p < 0.001$, ISI-shuffling test.

(E) Distribution of the preferred stimulus for every task, and pooled over all tasks together ("Total") of all 181 social-place-remapping units. Stim 1 is the "social" stimulus, and Stim 2 is the reference animal (male, group-housed, non-stressed). For each stimulus, the unit number is indicated. Error bars, binomial errors.

(F) Prevalence of social-place-remapping units (k) out of the total number of units recorded from every PFC subregion (n). Error bars, binomial errors. p_{mc}, Monte Carlo-based odds of obtaining a social-place-remapping unit by chance. Dashed line, the population mean. $^{*}p < 0.01$.

(G) Bias-corrected spatial MI vs. social MI values for all 181 social-place-remapping units. P_U, Mann-Whitney U test p value. Red dot corresponds to the unit in (A–D). Ellipse, 95% confidence interval. Plus sign, mean ± SD. cc, rank-order correlation coefficient.

(H–N) All conventions are the same as in panels (A–G), but for the social-place-coding group of units. $^{*}/^{**}p < 0.01/0.001$, chi-squared test.

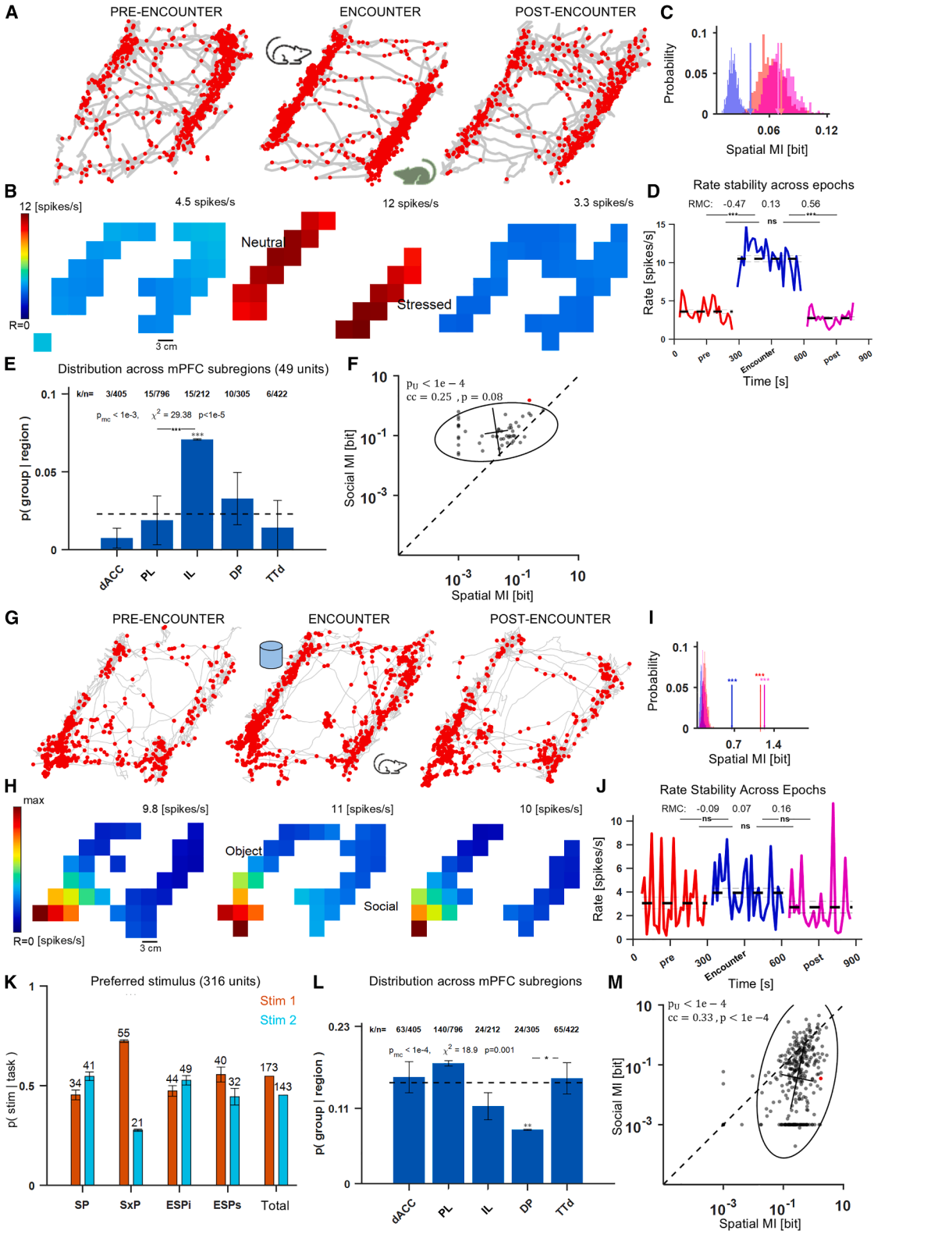

(legend on next page)

stimulus chamber during the pre-encounter and post-encounter epochs (2,002/2,042 spikes, 98%), while preferring the left chamber during the encounter epoch (780/889 spikes, 88%; Figure 4A). The same pattern is evident in the corresponding rate maps (Figure 4B). As shown in the rate map of the encounter epoch (Figure 4B, middle panel), this unit showed spatial preference for the side of the Lego (object) stimulus over the animal (social) stimulus. To establish that the unit exhibits spatial modulation during all three epochs, the spatial MI during each epoch was compared to chance using ISI shuffling. The bias-corrected spatial MI ranged from 0.61 to 0.88 bits ($p < 0.001$ during all three epochs; Figure 4C).

Next, the effect of the social stimuli on the mean firing rate of the unit was quantified. For that, we compared the RMC values for each pair of epochs (Figure 4D). The rate decreased after the pre-encounter epoch (RMC = 0.24, $p < 0.001$; ISI-shuffling test) and increased after the encounter epoch (RMC = −0.23, $p < 0.001$). This suggests that this specific unit also exhibited a rate modulation due to the presence of a social stimulus. Of the 225/2,140 units that showed mean firing rate modulation only during the encounter epoch (RMC analysis; Figure 3F), 19 units (10.5%) were social-place-remapping units.

The pattern of reversing spatial preferences during the presentation of the social stimuli, i.e., the same preference during the pre-encounter and post-encounter epochs but opposite preference during the encounter epoch, was observed in 181/2,140 (8.5%) units. We refer to these units as ''social-place-remapping'' units. This pattern is distinct from pure spatial preference and suggests that the spatial remapping may be due to the presence of social stimuli during the encounter epoch. Additional examples of social-place-remapping units, recorded from different mice during the various social tasks, are presented in Figures S4A–S4D.

The probabilities of all preferred stimuli during every task for all 181 social-place-remapping units were examined (Figure 4E). Chi-squared tests were applied to each pair of probabilities to estimate whether they differ, and no statistical difference was observed across stimuli and tasks. This suggests that place remapping is not a predominant shift to the side of the specific social stimulus, but is induced by the social context.

The distribution of units in the social-place-remapping group among the different subregions of the PFC is presented in Figure 4F. The analysis addressed two distinct questions. The first question was whether the prevalence of social-place-remapping units is as expected (regardless of a specific brain site). To answer this question, we used a Monte Carlo technique to derive a large dataset (20 repetitions, 2,140 units per repetition) from the original data but with ISI-shuffled spike times. The exact same classification pipeline was used to estimate the odds of obtaining a social-place-remapping unit by chance. The mean prevalence of social-place-remapping units in the ISI-shuffled datasets was 0/2,140, yielding a very low empirical probability ($p_{mc} < 0.0001$). Thus, when units from all subregions are pooled together, the observed prevalence is higher than expected by chance. This indicates that although the prevalence of social-place-remapping units is only 8.5%, it is substantial.

Second, we tested the null hypothesis that the prevalence of social-place-remapping units among PFC subregions is uniform (Figure 4F). We found that the distribution is not uniform ($p = 0.002$, chi-squared test). Rather, a dorsoventral decrease in prevalence was observed from the dACC to the DP. Post hoc analysis revealed an overrepresentation of social-place-remapping units in the dACC ($p = 0.003$, binomial test). The analysis was conducted by calculating a binomial success rate representing the probability of observing a social-place-remapping unit in a given subregion, given a chance level (under the null hypothesis, i.e., the population mean). We further compared representations between two specific pairs of subregions: the PL vs. IL and the DP vs. TTd. The PL and IL are the most studied subregions of the rodent PFC and were linked by multiple studies to distinct, sometimes opposite roles in various behaviors, including social behavior.[29] In contrast, the DP and TTd are relatively unexplored regions often considered olfactory-related and were recently linked to psychosocial stress[30] and affective behavior.[31] In both cases, chi-squared tests were applied to the prevalence of social-place-remapping units, and no statistical differences were found.

We calculated social and spatial MI values to compare the social and spatial components of the social-place-remapping units. For every unit, the spatial MI was computed between the spike train that spanned the entire three epochs and animal position (as in Figures 3B–3E, and 4C, yet for all three epochs together). The social MI was computed based on the same spike train, but with a binary variable indicating whether there were social stimuli in the environment. Both MIs were de-biased to allow fair comparison. Units that exhibit higher spatial MI also exhibit higher social MI (cc, 0.28; $p < 0.001$, permutation test), with higher spatial MI (median [IQR], 0.25 [0.12, 0.53] bit) than social MI (0.04 [0, 0.21] bit; $p < 0.001$, Mann-Whitney U test; Figure 4G).

Thus, the group of social-place-remapping units demonstrates the social aspect of spatial coding in two ways: by place remapping, i.e., the change in neuronal spatial preference during the encounter epoch only (observed in all 181 units), and by the rate-modulation, i.e., the change in mean firing rate during the encounter epoch only (observed in 19 units).

Place coding is induced in the presence of social stimuli

In another group, spatial coding was limited to the encounter epoch. An example unit recorded during an SP task (Figures 4H–4K and S3B) fired only a few spikes during the pre-encounter and post-encounter epochs (Figures 4H and 4I, left and right panels). However, during the encounter epoch, spikes were emitted in proximity to the social stimulus chamber, but not near the object chamber (Figures 4H and 4I, middle).

Figure 5. Rate modulation is induced during the presence of social stimuli and PFC units with stable-spatial-preference over epochs

(A–F) An example (A–D) and population analysis (E–F) of the social-rate-modulation group of units. All conventions are the same as in Figures (4A–4D), (4F), and (4G). ***$p < 0.0001$, chi-squared test.

(G–M) All conventions are the same as in Figures (4A–4G), but for the stable-spatial-preference group of units.

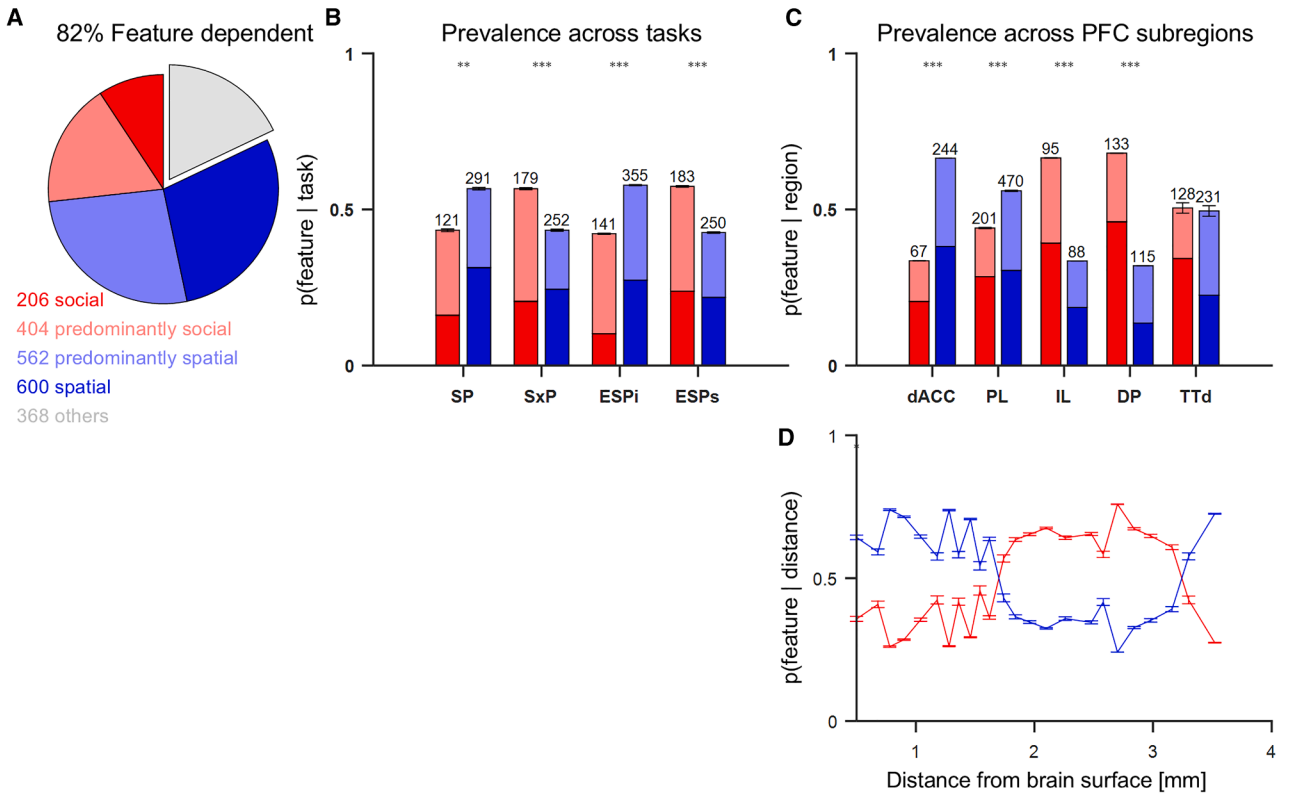

Figure 6. The distribution of social and spatial units exhibits a dorsoventral gradient along the PFC

(A) Partitioning all 2,140 units into "feature dependent" and non-feature dependent, according to the MI analysis.

(B) Distribution of feature-dependent units given a task using the same color code as in (A). Numbers indicate the total units recorded during every task. Error bars, binomial errors. **/***$p < 0.001/0.0001$, indicating the probability of the corresponding social and spatial representations being similar.

(C) Same as (B) for PFC subregions. (D) Same as (C), partitioning units according to the distance from the brain surface. Mean ± SD bin size, 0.14 ± 0.05 mm.

Accordingly, the spatial MI for this unit was above chance only during the encounter epoch ($p < 0.001$; Figure 4J, blue histogram). The mean firing rates were similar during the pre-encounter and post-encounter epochs (0.13 and 0.12 spikes/s) and higher during the encounter epoch (1.3 spikes/s; $p < 0.001$; Figure 4K). We observed 140/2,140 (6.5%) units, which we refer to as "social-place-coding" units (additional examples in Figures S4E–S4H).

Although both isolation and stress are associated with an affective state, the distribution of the preferred stimulus across tasks for the social-place-coding units showed an opposite trend in the ESPi and ESPs tasks (Figure 4L). While the naive stimulus (stimulus 2 in the ESPi task) was preferred in the ESPi task, the stressed stimulus (stimulus 1 in the ESPs task) was preferred during the ESPs task.

The null hypothesis that social-place-coding units distribute uniformly among the PFC subregions was rejected ($p = 0.032$, chi-squared test; Figure 4M). An over-representation of social-place-coding units was observed specifically in the DP (31 social-place-coding units out of 306 units recorded from the DP; $p = 0.008$, binomial test).

We found that the social and spatial MI values of social-place-coding units were correlated (cc, 0.6; $p < 0.001$, permutation test). However, on a unit-by-unit basis, the social MI (median [IQR], 0.047 [0.01, 0.19] bit) did not differ from the spatial MI (0.06 [0.02, 0.15] bit; $p = 0.73$, Mann-Whitney U test; Figure 4N). Overall, we observed a group of PFC—specifically DP— units that exhibit spatial coding only when social stimuli are present, with stimulus-specific preferences in the ESP paradigms.

Rate modulation is induced in the presence of social stimuli

The third group of units displayed spiking activity that was uniform in space during all three epochs, i.e., did not exhibit place preference during any epoch. While the firing rates were similar during the pre-encounter and post-encounter epochs, they were distinct during the encounter epoch. Thus, these units showed modulation of the mean firing rates, which was induced only during the presence of social stimuli in the experimental arena. We refer to this group as "social-rate-modulation" (Figures 5A–5F and S5A–S5D). Notably, this group is a subset of the 225 rate-modulated units (Figure 3F, blue dots) that had no spatial preference during any epoch. A total of 49/2,140 (2.3%) social-rate-modulation units were recorded. Of these, 31/49 (63%) showed a rate increase during the social encounter epoch, while the firing rates of the other 18 decreased during the social encounter.

In an example unit (Figures 5A–5D and S3C) recorded during the ESPs task, the firing patterns were distributed uniformly across space during all three epochs. Nevertheless, the uniform patterns exhibit low rates during the pre-encounter (mean, 4.5 spikes/s) and post-encounter (3.3 spikes/s) epochs (Figure 5B) and higher rates (11.7 spikes/s) during the encounter epoch (Figure 5D). The uniform patterns are corroborated by the low spatial MI values during all three epochs (within chance levels; Figure 5C).

By definition, the social-rate-modulation units do not have a preferred stimulus. Their prevalence across tasks did not differ from a uniform distribution ($p = 0.23$, chi-squared test). In contrast, the distribution over PFC subregions differed ($p < 0.0001$; Figure 5E). Specifically, social-rate-modulation units were overrepresented in the IL, compared with the population mean ($p < 0.0001$, binomial test; dashed line in Figure 5E) and compared with the PL ($p < 0.0001$, chi-squared test). The increase in social-rate-modulation units ventrally in the PFC does not contradict the decrease of social-place-remapping units in those subregions, as the two groups are mutually exclusive.

Since the social-rate-modulation units exhibit low spatial information values by definition, they may be considered the "most socially oriented" among all previously described groups. Indeed, almost all units in this group had higher social MI (median [IQR], 0.1 [0.07, 0.22] bits) than spatial MI (0.02 [0, 0.06] bits; $p < 0.0001$, U test; Figure 5F). The MI values did not correlate with each other (cc, 0.25; $p = 0.08$, permutation test).

PFC units with stable-spatial-preference over epochs

Finally, we observed that some PFC units exhibit stable spatial preference across the different epochs, akin to "classical" hippocampal place cells. Over all mice and tasks, we found 316/2,140 (14.8%) units with stable-spatial-preference. Examples are shown in Figures 5G–5M and S5E–S5H. For each "stable-spatial-preference" unit, spatial MI was above chance during all three epochs. Nevertheless, even in this spatial group, an impact of the social stimuli was observed, as in 40/316 (13%) of the units, epoch-dependent rate modulation was also observed (RMC test, $p < 0.05/3$, Bonferroni corrected for multiple comparisons).

In an example unit recorded during the SP task (Figures 5G–5J and S3D), spiking activity (Figures 5G and 5H) was observed predominantly when the animal was at the bottom left corner of the arena, during all three epochs. During all three epochs, spatial MI was higher than chance level (Figure 5I). While the firing rate was slightly higher during the encounter epoch (Figure 5J, blue), the spatial MI was lower during this epoch compared with the two other epochs.

At the group level, the distribution of the preferred stimuli across tasks was more prominent only in the SxP task, where the female stimulus side was preferred over the male (stimulus 1 in the SxP task; $p < 0.0001$, chi-squared test; Figure 5K). This does not imply a causal link between the social stimuli and spatial coding. That is, since the direct social effect cannot be separated from the general spatial preference observed already before the social encounter for the SxP units that exhibited stable-spatial-preference.

The odds of obtaining stable-spatial-preference units in all subregions of the PFC were found to be above chance (mean expected number: 0/2140; $p_{mc} < 0.0001$; Figure 5L). The distribution of these units among the PFC subregions differed from uniform ($p = 0.001$, chi-squared test; Figure 5L). As in the social-place-remapping group, subregion-specific prevalence decreased dorsoventrally, with the lowest representation in the DP (24/305 units). Comparing the subregion-specific probabilities of observing a stable-spatial-preference unit to the population mean showed under-representation in the DP ($p < 0.001$, chi-squared test; Figure 5L) and the TTd ($p = 0.002$).

By definition, units in the stable-spatial-preference group exhibited higher spatial MI values (median [IQR], 0.33 [0.18, 0.59] bit) compared with social MI (0.05 [0, 0.24] bit; $p < 0.001$, U test; Figure 5M). The two MI values were correlated (cc, 0.33; $p < 0.0001$, permutation test). Nevertheless, many units in the group exhibited a strong social effect, i.e., rate-modulation during the encounter epoch; in some cases, the two MI values were similar. This resembles the rate-remapping phenomenon observed in the hippocampus,[32] where the place fields do not shift but the rate changes. In the stable-spatial-preference group, the rate modulation of 40/316 units may be due to the presence of social stimuli in the arena.

The distribution of social and spatial units exhibits a dorsoventral gradient along the PFC

Since a mixture of social and spatial patterns was observed in the neuronal activity, we quantified the effect sizes at the population level (2,140 units). For every unit, we compared the social and spatial MI values to shuffled values, obtaining two p values (as in Figure 4G) that indicate whether the social and spatial MI were above chance ($p < 0.05/2$, Bonferroni correction for multiple comparisons). If either MI value was significant, the unit was denoted "feature-dependent." We found that 1,772/2,140 (82.8%) of the units were feature-dependent (Figure 6A).

Next, we classified the feature-dependent units as "social" or "spatial" if only one p value passed the threshold. If both p values passed, we classified the unit as "predominantly social" or "predominantly spatial" according to the higher MI value. The number of social units classified using this analysis ($n = 206$) was very close to the number found by the RMC analysis ($n = 225$; Figure 3F). Similar results were obtained using an independent generalized linear model (GLM) analysis (Table S2).

The prevalence of feature-dependent social and spatial units was analyzed according to social tasks and PFC subregions (Figures 6B and 6C). For each analysis, the number of social (or predominantly social) units was compared with the number of spatial (or predominantly spatial) units. The numbers for each category were scaled by the total number of social or spatial units. We found that across tasks (Figure 6B), social units were more prominent in the SxP ($p < 0.001$, chi-squared test) and ESPs ($p < 0.0001$) tasks. In contrast, spatial units were more prominent in the SP ($p < 0.001$) and ESPi ($p < 0.0001$) tasks. This suggests an additional difference observed between the two flavors of the ESP paradigm.

One of the most interesting results observed was the distribution of social and spatial units across the different PFC subregions (Figure 6C). While the prevalence of social units increased

gradually from the dACC to the DP, an opposite gradient was observed dorsoventrally for the spatial units. The only region that deviated from this pattern was the TTd, where the prevalence of social and spatial units appeared similar. Further, a clear preference for spatial representation was observed in the dACC ($p < 0.0001$, chi-squared test) and PL ($p < 0.0001$), and vice versa for the IL cortex ($p < 0.0001$) and the DP ($p < 0.0001$). This corroborates the independent analyses carried out for each group (Figures 4F, 4M, 5E, and 5L), suggesting a gradient of social vs. spatial representation across the dorsoventral axis of the PFC. Similar results were observed while grouping units according to distance from the brain surface (Figure 6D). Specifically, the prevalence of spatial units was higher in closer to the surface, and vice versa for the social units (excluding the deepest area).

Overall, the findings indicate opposing social and spatial coding gradients along the dorsoventral axis of the mouse PFC, with spatial coding decreasing and social coding increasing dorsoventrally from the ACC to the DP.

DISCUSSION

Space representation by cognitive maps in the brain was extensively explored during the last half-century.[33,34] Research revealed many functional cell types encoding various spatial features, including place, grid, border, head direction, and object vector cells. These cell types were primarily observed in the hippocampal formation.[35] More recently, a growing body of evidence suggests spatial neuronal representations in brain regions beyond the hippocampal formation.[36] Specifically, multiple studies associate spatial memory with the PFC.[37,38] This forebrain region is involved in decision-making and trajectory planning,[16,17] as well as in social and emotional behaviors in general and specifically in recognizing affective states or others.[22,24,39]

The organization of space according to social considerations is crucial for the survival of any species, including humans.[40] This ability underlies socially based spatial decision-making, such as planning a trajectory among individuals and aiming to hold or avoid specific social interactions.[9] Moreover, sociospatial abilities are crucial for territorial behavior,[14] where an individual claims an area and defends it against conspecifics.[41] Territorial behavior requires dividing space into self-territory and the territories of other individuals, requiring the integration of social and spatial information in the brain. Notably, seminal work[25] demonstrated that nucleus accumbens-projecting PL PFC neurons encode a combination of social and spatial information during navigation within a social context.

Here, we analyzed neuronal activity over the dorsoventral axis of the PFC while the recorded mice conducted several distinct social discrimination tasks. Notably, while the social context varied between tasks, the spatial context remained fixed. The various observed distributions of neuronal spatial preferences support context-dependent representation of the space by PFC neuronal activity.[42]

Multiple single units changed their spatial firing pattern specifically during the social encounter epoch, suggesting a direct relationship between the two factors. We classified the units according to the type of change observed in their firing patterns. In one group of PFC units (Figures 4A–4G), spatial modulation remapped during the encounter session, exemplifying how the presence of conspecifics may alter the representation of space. In a second group of PFC units (Figures 4H–4N), the spatial preference was evident only during the social encounter epoch. A similar social code of others, which differs from self-place coding, was reported in the bat hippocampus[11] and CA1 of female mice.[12] Interestingly, units in this group had distinct preferences for different affective states. This finding aligns with our previously reported results, where male mice distinguish between stressed and isolated conspecifics.[24]

In the third group of PFC units, no spatial modulation was observed (Figures 5A–5F), but rate modulation occurred only during the encounter epoch. These changes can be thought of as a binary indicator for whether social stimuli are apparent in the environment. This group was prominent mainly in the IL cortex, suggesting anatomical specialization. The fourth PFC group (Figures 5G–5N) included units resembling hippocampal place cells. These neurons were more spatial than social, but the firing rate of some units was modulated during the presence of social stimuli, resembling the rate-remapping phenomenon observed in the hippocampus.[32] Like the first group, the anatomical representation decreased dorsoventrally, with the lowest prevalence in the DP, even as compared with the TTd. Notably, the DP and TTd, which are often analyzed together,[30,31] exhibited distinct characteristics throughout our study. The fact that the TTd was not an integral part of the dorsoventral gradient may reflect its association with olfactory regions that receive direct inputs from the olfactory bulb, including the adjacent anterior olfactory nucleus.[43] In contrast, the DP, which does not receive such inputs,[44] was an integral part of the PFC dorsoventral gradient.

Overall, a mixture of social and spatial encoding schemes was observed (Figure 6), demonstrating various types of sociospatial modulations in firing patterns, some of which were stimulus-specific. Further research is required to determine whether single units are context-specific, for instance, by recording the same units during multiple tasks.

One of the most interesting observations of this study was the gradual change in the social and spatial components of firing patterns along the dorsoventral axis of the PFC (excluding the TTd; Figure 6C). While spatial units were more prevalent in dACC and PL, the prevalence of social encoding units was higher in IL and DP. This dorsoventral gradient in social vs. spatial information was observed not only for each of the four mutually exclusive groups (Figures 4 and 5) but also when all units were analyzed together and in two distinct manners (Figures 2E and 6C). The fact that the correlation between behavioral and neuronal representations exhibited the same gradient as the neuronal representation of space strongly supports the existence of anatomical-functional specialization. This conclusion is further supported by the results obtained when analyses were conducted according to distance from the brain surface (Figures 2F and 6D). Further, the gradients observed included the DP but not the TTd. This supports the contention that the DP and the TTd are functionally distinct.

A dorsoventral functional gradient in the mammalian PFC was associated with a general distinction between the "what" and the "where" already in 1983.[45] Ever since, a growing body of

work reported a similar gradient with different aspects of behavior and cognition (for comprehensive reviews, see Jabarin et al.[24] and Heidbreder et al. [46]), including attention to memory,[47] behavioral inhibition,[48] and decision making.[20] Notably, in accordance with our results, a recent study revealed that spatial MI is higher for units recorded in the dorsal vs. the ventral PFC.[37] The findings of the previous work,[37] focusing on spatial representation, compared spatial MI between two PFC parts, dorsal and ventral. Here, we complemented and extended these findings by focusing on socio-spatial representation and showing a gradient along five PFC subregions, as well as over distance from the brain surface, of both spatial and social MI.

Functional electrophysiology studies are supported by anatomical work, showing a gradient of PFC connections with the other brain regions. Specifically, the ventral PFC is connected more strongly to limbic structures and neuromodulatory centers, whereas the dorsal PFC is connected to motor and premotor areas.[49,50] These studies support the interpretation that ventral PFC subregions are more specialized for emotional control, whereas dorsal subregions are more specialized for the control of actions. Our results support this contention, suggesting that emotional social encoding is more prominent in ventral PFC, while spatial encoding, which is related to the control of action, is more prevalent in the dorsal PFC.

Limitations of the study

Several limitations of this study should be discussed. First, the mice were socially isolated after the implantation surgery, which may influence their behavior. However, our previous studies showed that acutely isolated mice perform the social discrimination tasks used here very similarly to group-housed mice.[23,24]

Second, the mice underwent brief (5–10 s) isoflurane anesthesia during connection to the recording system, followed by a 10-min habituation period before every recording session. This procedure is routinely used for electrophysiological and fiber photometry recordings to prevent animals from struggling during connection to the recording system.[22–24] While we have never noticed changes in social behavior following the isolation and isoflurane anesthesia procedures, the light anesthesia procedure may affect the recorded neural activity. Notably, the social behavior of the recorded animals, as carefully measured using unbiased computational methods,[51] was identical to the behavior measured from unimplanted animals.[52]

We used a red LED to illuminate the experimental arena, although mice cannot see red well. As nocturnal animals live in burrows, most of their natural social interactions are in the dark. Moreover, it was reported that in semi-natural conditions, laboratory mice show more social approach behavior in the dark phase, while spending more time in huddling during the light phase.[53] For these reasons, we are cautious in conducting all social behavior experiments in the dark phase under dim red light that does not disturb the circadian cycle of the animals or cause any light-driven anxiety.

Another limitation is the relatively small size of the arena and the relatively short duration of each epoch recorded, which restricts the amount of data collected. This reduces the ability to clearly identify the place fields of spatial units. To mitigate this limitation, we identified spatial units by comparing their spatial MI to chance MI generated by ISI shuffling each spike train while keeping the same behavior. This yielded 497/2,140 (23%) spatial units, which is similar to the prevalence of spatial representation reported in other PFC studies (e.g., 21% in Maisson et al.[54]).

A final limitation is that the sides of the stimuli, which were chosen randomly, were not swapped for a given mouse. This may make it difficult to fully separate the social and spatial aspects conjugated in the spiking activity of an individual unit and raises questions about the causality between the social stimuli and the observed remapping patterns. Nevertheless, our results repeatedly showed gradual patterns along the PFC using a large dataset of well-isolated units. Therefore, at the population level, our results can at least form a lower bound for socio-spatial gradients and interconnections in the PFC.

Overall, the results presented here shed new light on the dynamics of the social representation of space in the mammalian brain, which is crucial for social behavior in general and territorial behavior in particular.

RESOURCE AVAILABILITY

Lead contact

Further information and requests for resources should be directed to and will be fulfilled by the lead contact, Lear Cohen (learcohen1510@gmail.com).

Materials availability

This study did not generate new, unique reagents.

Data and code availability

- All data underlying the results are available at Zenodo: https://doi.org/10.5281/zenodo.16949237 and are publicly available as of the date of publication.
- All codes needed to recreate all figures and tables in this manuscript can be found on the same repository.
- Any additional information required to reanalyze the data reported in this paper is available from the lead contact upon request.

ACKNOWLEDGMENTS

This study was supported by the Rosetrees Trust (CF-2023-I-2_113 to E.S.), the Ministry of Science, Technology and Space of Israel (7393 to E.S. and 3-12068 to S.W.), the Israel Science Foundation (2220/22 to S.W.), the Ministry of Health of Israel (3-18380 for EPINEURODEVO to S.W.), the German Research Foundation (DFG) (SH 752/2-1 to S.W.), the Congressionally Directed Medical Research Programs (CDMRP) (AR210005 to S.W.), the United States-Israel Binational Science Foundation (2019186 to S.W.), and the HORIZON EUROPE European Research Council (ERC-SyG oxytocINspace).

AUTHOR CONTRIBUTIONS

Conceptualization, E.S., L.C., S.N., and S.W.; data curation, A.N.M., L.C., and S.N.; formal analysis, L.C.; funding acquisition, S.W. and E.S.; investigation, A.N.M. and L.C.; methodology, L.C. and S.N.; project administration, S.N. and S.W.; resources: S.N.; software, L.C. and S.N.; supervision, E.S. and S.W.; validation: E.S.; visualization, L.C.; writing – original draft, L.C.; and writing – review & editing, A.N.M., E.S., S.N., and S.W.

DECLARATION OF INTERESTS

The authors declare no competing interests.

STAR★METHODS

Detailed methods are provided in the online version of this paper and include the following:

- KEY RESOURCES TABLE
- EXPERIMENTAL MODEL AND STUDY PARTICIPANT DETAILS
  - Animals
  - Experimental setup
- METHOD DETAILS
  - Behavioral paradigms
  - Social preference (SP) task
  - Sex preference (SxP) task
  - Emotional state preference (ESP) tasks
  - Surgery
  - *In vivo* electrophysiological recordings
- QUANTIFICATION AND STATISTICAL ANALYSIS
  - Markerless pose estimation
  - Spike detection and sorting
  - Cell quality analysis
  - Histology and probe track imaging
  - Brain area registration based on histology
  - Firing rate by position maps
  - Inter-spike interval shuffling test
  - Asterisks definitions
  - Behavioral vs. neuronal preferences in socio-spatial space
  - Spatial preference analysis
  - Rate modulation contrast (RMC)
  - Classification of units into groups
  - Brain subregion analysis
  - Social and spatial information analysis
  - The extent of social effect on the population's neuronal activity
  - GLM analysis

SUPPLEMENTAL INFORMATION

Supplemental information can be found online at https://doi.org/10.1016/j.celrep.2025.116319.

Received: February 13, 2025
Revised: July 16, 2025
Accepted: August 29, 2025

REFERENCES

1. Moser, E.I., Kropff, E., and Moser, M.B. (2008). Place cells, grid cells, and the brain's spatial representation system. Annu. Rev. Neurosci. *31*, 69–89.
2. Geva-Sagiv, M., Las, L., Yovel, Y., and Ulanovsky, N. (2015). Spatial cognition in bats and rats: from sensory acquisition to multiscale maps and navigation. Nat. Rev. Neurosci. *16*, 94–108.
3. Payne, H.L., Lynch, G.F., and Aronov, D. (2021). Neural representations of space in the hippocampus of a food-caching bird. Science *373*, 343–348.
4. Cohen, L., Vinepinsky, E., Donchin, O., and Segev, R. (2023). Boundary vector cells in the goldfish central telencephalon encode spatial information. PLoS Biol. *21*, e3001747.
5. Whittington, J.C.R., McCaffary, D., Bakermans, J.J.W., and Behrens, T.E.J. (2022). How to build a cognitive map. Nat. Neurosci. *25*, 1257–1272.
6. Colgin, L.L., Moser, E.I., and Moser, M.B. (2008). Understanding memory through hippocampal remapping. Trends Neurosci. *31*, 469–477.
7. Sheintuch, L., Geva, N., Baumer, H., Rechavi, Y., Rubin, A., and Ziv, Y. (2020). Multiple maps of the same spatial context can stably coexist in the mouse hippocampus. Curr. Biol. *30*, 1467–1476.e6.
8. Sanders, H., Wilson, M.A., and Gershman, S.J. (2020). Hippocampal remapping as hidden state inference. eLife *9*, e51140.
9. Thompson, J.C., and Parkinson, C. (2024). Interactions between neural representations of the social and spatial environment. Phil. Trans. B *379*, 20220522.
10. Eichenbaum, H. (2015). The hippocampus as a cognitive map, of social space. Neuron *87*, 9–11.
11. Omer, D.B., Maimon, S.R., Las, L., and Ulanovsky, N. (2018). Social place-cells in the bat hippocampus. Science *359*, 218–224.
12. Zhang, X., Cao, Q., Gao, K., Chen, C., Cheng, S., Li, A., Zhou, Y., Liu, R., Hao, J., Kropff, E., and Miao, C. (2024). Multiplexed representation of others in the hippocampal CA1 subfield of female mice. Nat. Commun. *15*, 3702.
13. Danjo, T., Toyoizumi, T., and Fujisawa, S. (2018). Spatial representations of self and other in the hippocampus. Science *359*, 213–218.
14. Wirth, S., Soumier, A., Eliava, M., Derdikman, D., Wagner, S., Grinevich, V., and Sirigu, A. (2021). Territorial blueprint in the hippocampal system. Trends Cogn. Sci. *25*, 831–842.
15. El-Gaby, M., Harris, A.L., Whittington, J.C.R., Dorrell, W., Bhomick, A., Walton, M.E., Akam, T., and Behrens, T.E.J. (2024). A cellular basis for mapping behavioural structure. Nature *636*, 671–680.
16. Stout, J.J., and Griffin, A.L. (2020). Representations of on-going behavior and future actions during a spatial working memory task by a high firing-rate population of medial prefrontal cortex neurons. Front. Behav. Neurosci. *14*, 151.
17. Kaefer, K., Nardin, M., Blahna, K., and Csicsvari, J. (2020). Replay of behavioral sequences in the medial prefrontal cortex during rule switching. Neuron *106*, 154–165.e6.
18. Frost, N.A., Haggart, A., and Sohal, V.S. (2021). Dynamic patterns of correlated activity in the prefrontal cortex encode information about social behavior. PLoS Biol. *19*, e3001235.
19. Yizhar, O., Fenno, L.E., Prigge, M., Schneider, F., Davidson, T.J., O'shea, D.J., Sohal, V.S., Goshen, I., Finkelstein, J., Paz, J.T., et al. (2011). Neocortical excitation/inhibition balance in information processing and social dysfunction. Nature *477*, 171–178.
20. Diehl, G.W., and Redish, A.D. (2023). Differential processing of decision information in subregions of rodent medial prefrontal cortex. eLife *12*, e82833.
21. Lee, E., Rhim, I., Lee, J.W., Ghim, J.W., Lee, S., Kim, E., and Jung, M.W. (2016). Enhanced neuronal activity in the medial prefrontal cortex during social approach behavior. J. Neurosci. *36*, 6926–6936.
22. Mohapatra, A.N., and Wagner, S. (2023). The role of the prefrontal cortex in social interactions of animal models and the implications for autism spectrum disorder. Front. Psychiatry *14*, 1205199.
23. Mohapatra, A.N., Peles, D., Netser, S., and Wagner, S. (2024). Synchronized LFP rhythmicity in the social brain reflects the context of social encounters. Commun. Biol. *7*, 2.
24. Jabarin, R., Mohapatra, A.N., Ray, N., Netser, S., and Wagner, S. (2025). Distinct prelimbic cortex neuronal responses to emotional states of others drive emotion recognition in adult mice. Curr. Biol. *35*, 994–1011.e8.
25. Murugan, M., Jang, H.J., Park, M., Miller, E.M., Cox, J., Taliaferro, J.P., Parker, N.F., Bhave, V., Hur, H., Liang, Y., et al. (2017). Combined social and spatial coding in a descending projection from the prefrontal cortex. Cell *171*, 1663–1677.e16.
26. Fee, M.S., Mitra, P.P., and Kleinfeld, D. (1996). Variability of extracellular spike waveforms of cortical neurons. J. Neurophysiol. *76*, 3823–3833.
27. Schmitzer-Torbert, N., Jackson, J., Henze, D., Harris, K., and Redish, A.D. (2005). Quantitative measures of cluster quality for use in extracellular recordings. Neuroscience *131*, 1–11.
28. Jeffery, K.J. (2011). Place cells, grid cells, attractors, and remapping. Neural Plast. *2011*, 182602.
29. Huang, W.C., Zucca, A., Levy, J., and Page, D.T. (2020). Social behavior is modulated by valence-encoding mPFC-amygdala sub-circuitry. Cell Rep. *32*, 107899.

30. Kataoka, N., Shima, Y., Nakajima, K., and Nakamura, K. (2020). A central master driver of psychosocial stress responses in the rat. Science *367*, 1105–1112.

31. Botterill, J.J., Khlaifia, A., Appings, R., Wilkin, J., Violi, F., Premachandran, H., Cruz-Sanchez, A., Canella, A.E., Patel, A., Zaidi, S.D., and Arruda-Carvalho, M. (2024). Dorsal peduncular cortex activity modulates affective behavior and fear extinction in mice. Neuropsychopharmacology *49*, 993–1006.

32. Leutgeb, S., Leutgeb, J.K., Barnes, C.A., Moser, E.I., McNaughton, B.L., and Moser, M.B. (2005). Independent codes for spatial and episodic memory in hippocampal neuronal ensembles. Science *309*, 619–623.

33. Poulter, S., Hartley, T., and Lever, C. (2018). The neurobiology of mammalian navigation. Curr. Biol. *28*, R1023–R1042.

34. Epstein, R.A., Patai, E.Z., Julian, J.B., and Spiers, H.J. (2017). The cognitive map in humans: spatial navigation and beyond. Nat. Neurosci. *20*, 1504–1513.

35. Moser, E.I., Moser, M.B., and McNaughton, B.L. (2017). Spatial representation in the hippocampal formation: a history. Nat. Neurosci. *20*, 1448–1464.

36. Maisson, D.J.N., Wikenheiser, A., Noel, J.P.G., and Keinath, A.T. (2022). Making sense of the multiplicity and dynamics of navigational codes in the brain. J. Neurosci. *42*, 8450–8459.

37. Sauer, J.F., Folschweiller, S., and Bartos, M. (2022). Topographically organized representation of space and context in the medial prefrontal cortex. Proc. Natl. Acad. Sci. USA *119*, e2117300119.

38. Churchwell, J.C., Morris, A.M., Musso, N.D., and Kesner, R.P. (2010). Prefrontal and hippocampal contributions to encoding and retrieval of spatial memory. Neurobiol. Learn. Mem. *93*, 415–421.

39. Xu, H., Liu, L., Tian, Y., Wang, J., Li, J., Zheng, J., Zhao, H., He, M., Xu, T.L., Duan, S., and Xu, H. (2019). A disinhibitory microcircuit mediates conditioned social fear in the prefrontal cortex. Neuron *102*, 668–682.e5.

40. Schafer, M., and Schiller, D. (2018). Navigating social space. Neuron *100*, 476–489.

41. Maher, C.R., and Lott, D.F. (1995). Definitions of territoriality used in the study of variation in vertebrate spacing systems. Anim. Behav. *49*, 1581–1597.

42. Hyman, J.M., Ma, L., Balaguer-Ballester, E., Durstewitz, D., and Seamans, J.K. (2012). Contextual encoding by ensembles of medial prefrontal cortex neurons. Proc. Natl. Acad. Sci. USA *109*, 5086–5091.

43. Bhattarai, J.P., Etyemez, S., Jaaro-Peled, H., Janke, E., Leon Tolosa, U.D., Kamiya, A., Gottfried, J.A., Sawa, A., and Ma, M. (2022). Olfactory Modulation of the Medial Prefrontal Cortex Circuitry: Implications for Social cognition. Semin. Cell. Dev. Biol. *129*, 31–39.

44. Hintiryan, H., Rudd, M., Nanda, S., Gutierrez, A., Lo, D., Boesen, T., Garcia, L., Sun, J., Estrada, C., Mun, H.S., et al. (2025). Distinct subnetworks of the mouse anterior thalamic nuclei. Nat. Commun. *16*, 6018.

45. Mishkin, M., Ungerleider, L.G., and Macko, K.A. (1983). Object vision and spatial vision: two cortical pathways. Trends Neurosci. *6*, 414–417.

46. Heidbreder, C.A., and Groenewegen, H.J. (2003). The medial prefrontal cortex in the rat: evidence for a dorso-ventral distinction based upon functional and anatomical characteristics. Neurosci. Biobehav. Rev. *27*, 555–579.

47. Cassaday, H.J., Nelson, A.J.D., and Pezze, M.A. (2014). From attention to memory along the dorsal-ventral axis of the medial prefrontal cortex: some methodological considerations. Front. Syst. Neurosci. *8*, 160.

48. Hardung, S., Epple, R., Jäckel, Z., Eriksson, D., Uran, C., Senn, V., Gibor, L., Yizhar, O., and Diester, I. (2017). A functional gradient in the rodent prefrontal cortex supports behavioral inhibition. Curr. Biol. *27*, 549–555.

49. Gabbott, P.L.A., Warner, T.A., Jays, P.R.L., Salway, P., and Busby, S.J. (2005). Prefrontal cortex in the rat: projections to subcortical autonomic, motor, and limbic centers. J. Comp. Neurol. *492*, 145–177.

50. Hoover, W.B., and Vertes, R.P. (2007). Anatomical analysis of afferent projections to the medial prefrontal cortex in the rat. Brain Struct. Funct. *212*, 149–179.

51. Netser, S., Haskal, S., Magalnik, H., Bizer, A., and Wagner, S. (2019). A system for tracking the dynamics of social preference behavior in small rodents. JoVE J. *2019*, e60336.

52. Kopachev, N., Netser, S., and Wagner, S. (2022). Sex-dependent features of social behavior differ between distinct laboratory mouse strains and their mixed offspring. iScience *25*, 103735.

53. Arakawa, H., Blanchard, D.C., and Blanchard, R.J. (2007). Colony formation of C57BL/6J mice in visible burrow system: identification of eusocial behaviors in a background strain for genetic animal models of autism. Behav. Brain Res. *176*, 27–39.

54. Maisson, D.J.N., Cervera, R.L., Voloh, B., Conover, I., Zambre, M., Zimmermann, J., and Hayden, B.Y. (2023). Widespread coding of navigational variables in prefrontal cortex. Curr. Biol. *33*, 3478–3488.e3.

55. Mathis, A., Mamidanna, P., Cury, K.M., Abe, T., Murthy, V.N., Mathis, M.W., and Bethge, M. (2018). DeepLabCut: markerless pose estimation of user-defined body parts with deep learning. Nat. Neurosci. *21*, 1281–1289.

56. Montijn JS, Heimel JA. A universal pipeline for the alignment of electrode tracks with slice histology and electrophysiological data. Preprint at bioRxiv https://doi.org/10.1101/2022.06.20.496782.

57. Someck, S., Levi, A., Sloin, H.E., Spivak, L., Gattegno, R., and Stark, E. (2023). Positive and biphasic extracellular waveforms correspond to return currents and axonal spikes. Commun. Biol. *6*, 950.

58. Wang, Q., Ding, S.L., Li, Y., Royall, J., Feng, D., Lesnar, P., Graddis, N., Naeemi, M., Facer, B., Ho, A., et al. (2020). The Allen mouse brain common coordinate framework: a 3D reference atlas. Cell *181*, 936–953.e20.

59. Stark, E., and Abeles, M. (2005). Applying resampling methods to neurophysiological data. J. Neurosci. Methods *145*, 133–144.

60. Skaggs, W., Mcnaughton, B., and Gothard, K. (1992). An information-theoretic approach to deciphering the hippocampal code. Adv. Neural Inf. Process. Syst. *5*, 1031–1037.

61. Stark, E., Globerson, A., Asher, I., and Abeles, M. (2008). Correlations between groups of premotor neurons carry information about prehension. J. Neurosci. *28*, 10618–10630.

STAR★METHODS

KEY RESOURCES TABLE

REAGENT or RESOURCE	SOURCE	IDENTIFIER
Chemicals, peptides, and recombinant proteins		
Ketamine	Zoetis Inc. Spain	507340
Isoflurane	Piramal Critical Care Inc., USA	105-52-28997-00
Duratears	Alcon Couvreur N.V., Belgium	109-33-24050-00
Dental Cement	Unifast, GC America	GC-5150316
Meloxicam	Norbrook Laboratories Ltd, Ireland	150-41-33607-00
Baytril 5%	Elanco Animal Health GMBH	082-15-91819-00
Paraformaldehyde	Sigma	818708
DAPI (fluoroshield with DAPI)	Abcam	ab104139
Dil Stain (1,1′-Dioctadecyl-3,3,3′,3′-Tetramethylindocarbocyanine Perchlorate)	Sigma	42364
Deposited data		
Zenodo	–	https://doi.org/10.5281/zenodo.16949237
Experimental models: Organisms/strains		
CD-1	Envigo RMS, Israel	N/A
Software and algorithms		
Track Rodent	Netser et al.[51]	https://doi.org/10.3791/60336
Deeplabcut	Mathis et al.[55]	https://doi.org/10.1038/S41593-018-0209-Y
Kilosort 2.5	https://github.com/MouseLand/Kilosort	–
Phy	https://github.com/cortex-lab/phy	–
In-house MATLAB custom code	–	–
FlyCapture2	FLIR	FlyCap2Viewer_2.13.3.61_x64.exe
SpikeGLX	https://billkarsh.github.io/SpikeGLX/	Release_v20220101-phase30
Universal Probe Finder	Montijn et al.[56]	https://doi.org/10.1101/2022.06.20.496782
Other		
Neuropixels 1.0 PXIe acquisition system	IMEC, Belgium	PXIe_1000 + HST_1000
PXIe-1071 Express Chassis instrument	National Instruments	PXIe-1071
PXIe-6341 card	National Instruments	PXIe-6341
Flea3 USB3 camera	FLIR	FL3-U3-13E4M-C
Neuropixels 1.0 probes with cap	IMEC, Belgium	PRB_1_4_0480_1_C
In-house custom-made 3D-printed probe holder	–	–
silver wire	A-M Systems, Carlsborg, WA	–

EXPERIMENTAL MODEL AND STUDY PARTICIPANT DETAILS

Animals

The subject mice were five adult male ICR (CD-1, 8-18 week-old; Envigo RMS, Israel) mice (32–38 g). Stimulus mice were adult male and female ICR (CD-1, 8-18 week-old). Because we used only adult male ICR mice as experimental subjects, future work is required to generalize the study to other age, sex, and strains. Animals were kept in groups of 2–5 sex-matched animals per cage, with two exceptions. First, animals implanted with Neuropixels probes were kept isolated in a separate cage to keep their implants intact. Second, stimulus mice for the ESPi task were isolated 1–2 weeks before the experiment. All animals were housed at the animal facility of the University of Haifa under veterinary supervision, in an inverted 12 h light-dark cycle (lights on at 9 p.m.), with free access to water and food (standard chow diet, Envigo RMS, Israel). All experiments were performed according to the

National Institutes of Health guide for the care and use of laboratory animals and approved by the Institutional Animal Care and Use Committee of the University of Haifa (IACUC #UoH-IL-2301-103-4).

Experimental setup

Experiments were conducted during the dark phase of the dark/light cycle (human daytime) in a sound- and electromagnetic noise-attenuated cabinet (60 × 65 × 80 cm; L x W x H) grounded to the ground of the recording system and illuminated by a dim red LED strip placed at the top of inner walls of the cabinet.

The experimental setup[51] consisted of a black Plexiglas arena (37 × 22 × 35 cm) placed in the middle of the cabinet. To introduce the animal or Lego toy stimuli, two black Plexiglas triangular chambers (right-angled isosceles, 12 cm sides, 35 cm height) were placed at two randomly selected opposite corners of the arena. A metal mesh (12 × 6 cm, 1 × 1 cm holes) placed at the bottom of the triangular chamber allowed direct interaction of the implanted animal with the stimulus. A monochromatic camera (resolution, 1280x1024 pixels; mean ± SD frame rate, 30.02 ± 0.05 fps; Flea3 USB3, FLIR) equipped with a wide-angle lens was placed at the top of the acoustic cabinet and connected to a computer, enabling a clear view of stimulus chambers and the floor of the arena while recording subject behavior using commercial software (FlyCapture2, FLIR).

METHOD DETAILS

Behavioral paradigms

For every animal, the order of the tasks was randomized between days. Each animal participated in four tasks that included different stimulus sets (social contexts), two in the morning and two in the afternoon (Table S3). All stimuli used for each mouse were novel. Every task was considered a separate session. Before the first session, the recorded animal was placed for 5–10 s in a glass container containing a cotton swab with a drop of isoflurane to prevent the subject from struggling during the connection of the recording cable. The connected mice were then placed in the arena for a habituation period of 10 min. Then, two sessions were performed consecutively, separated by a 10-min interval. Each session (task) lasted 15 min and included three epochs: a 5-min pre-encounter epoch with an empty chamber, a 5-min encounter epoch with stimuli in the chambers, and an additional 5-min post-encounter epoch with empty chambers. Social stimuli were located in their chambers outside the acoustic cabinet for acclimation throughout the time before the encounter epoch. The full details of all experimental sessions and the timeline are presented in Table S3.

Social preference (SP) task

After the 5-min pre-encounter epoch, the two empty triangular chambers were replaced with chambers containing the social (adult male group-housed mouse) and object (Lego toy) stimuli, and the SP task was conducted for 5 min. Then, the stimulus-containing chambers were replaced with empty chambers for the 5-min post-encounter epoch.

Sex preference (SxP) task

The SxP task was conducted precisely in the same manner as the SP task. The only difference was that the second stimulus was an adult female mouse instead of a Lego toy.

Emotional state preference (ESP) tasks

The ESP tasks were conducted as the SP and SxP tasks, with the difference that the second stimulus was an additional male mouse associated with an affective state. These affective stimuli mice were either a socially isolated (1–2 weeks) animal, yielding the ESP isolated (ESPi) task, or a stressed animal, yielding the ESP stressed (ESPs) task. The latter were stressed by confinement to a 50 mL tube pierced with multiple ventilation holes for 15 min immediately before being introduced into the triangular chamber for 5 min of habituation, followed by stimulus introduction to the arena.

Surgery

For chronic electrophysiology experiments, every animal was implanted with a single Neuropixels 1.0 probe (NP1, #PRB_1_4_0480_1_C; IMEC, Belgium). The probe was assembled in a custom-made 3D-printed holder, and the reference and ground wires were soldered to the insulation-stripped ends of silver wires (ID, 127 μm; 300–500 Ω; A-M Systems, Carlsborg, WA). Before surgery, the probe shank was soaked in fluorescent DiI (42364; Sigma-Aldrich) for 10 min. The mice were anesthetized by isoflurane (induction 3%, 0.5%–0.8% maintenance in 200 mL/min air; SomnoSuite) and placed over a custom-made heating pad (37°C) under a stereotaxic device (Kopf Instruments, Tujunga, CA). Two watch screws (0–80, 1/16″) were inserted into the temporal bone to support the custom NP1 holder with dental cement. For implantation, the probe-containing holder was attached to a stereotaxic arm and centered at ML -0.4 mm, AP -1.9 mm relative to bregma after drilling the skull at this site to expose the dura (diameter, 0.5 mm). To angle the probe in two axes, the skull was given a pitch angle of 5° by raising the bregma 0.5 mm with respect to lambda, and a roll angle of 10° by rotating the snout holder. The reference and ground wires were inserted into respective burr holes drilled into the bone above the right hemisphere. Then, the probe was lowered to DV -4.6 mm, relative to bregma, at a rate of about 0.01 mm/s. A 50:50 w/w mix of petroleum oil and bone wax jelly was heated and poured gently to fill the craniotomy.

Dental cement was applied to the base of the NP1 holder and the two skull screws. The mice were injected with meloxicam (10 mg/kg) and enrofloxacin (15 mg/kg) to relieve pain and prevent infections for three days following surgery. Experimental sessions began four days after surgery.

In vivo electrophysiological recordings

All experiments were conducted in the experimental arena. Data from the NP1 probe were written into two separate binary files: one containing a high-pass filtered signal (“action potentials”: 0.3 to 10 kHz band, 30 kHz sampling rate, ×500 gain); and another containing a lower band signal (“LFP”: 0.5–500 Hz band, 2.5 kHz sampling rate, ×250 gain). Data were digitized on the headstage (10 bits, digitization range, 2.34375 μV/bit) using SpikeGLX (https://billkarsh.github.io/SpikeGLX/) through an IMEC board installed within a PXIe-1071 Express chassis (National Instruments). The camera timestamps were recorded through a PXIe-6341 card installed within the same chassis (National Instruments) at 25 kHz to synchronize the video with the neural recordings.

QUANTIFICATION AND STATISTICAL ANALYSIS

Markerless pose estimation

DeepLabCut (DLC[55]) software v.2.3.5 was used to track the positions of the mice during various tasks. The training set included 2379 frames (sampled at 30 fps) from 6 out of 20 sessions. The following body parts were marked manually, by a single experimenter (ANM), in each frame of training data: Left_ear, Right_ear, Nose, Center (of the neck), Lateral_left (of the body), Lateral_right (of the body), Tail_base, and Tail_end. The model was trained by 2 million iterations with the default DLC parameters (training frames selected by K-means clustering of each of the six videos, trained on 95% of labeled frames, initialized with dlcrnet_ms5, batch size of 8). The subject’s position was estimated using the center of the head (“Head_Center”), which was calculated as the center of the triangle composed of three body parts: the left ear, the right ear, and the nose.

Spike detection and sorting

Spiking band data acquired from SpikeGLX (high-pass filtered binary files, 0.3–10 kHz) were sorted into spike clusters automatically using Kilosort 2.5 (KS 2.5, https://github.com/MouseLand/Kilosort). The sorted spikes were manually curated, and noise clusters were removed using phy (https://github.com/cortex-lab/phy). Single-unit candidates were identified by eye according to the following criteria: Less than 0.1% of spikes had ISIs shorter than 2 ms, and spike waveforms appeared to be consistent with a single unit. Waveforms, auto-correlation histograms, and cross-correlation histograms of nearby units were compared to verify visually that no two clusters corresponded to the same neuron. Units that did not pass these criteria were tagged as multi-units. Out of the initial databases of 4189, the manual curation process yielded 2975 single-unit candidates.

Cell quality analysis

Next, to quantify the isolation quality of the single-unit candidates, we employed four metrics (Figure S1).

(1) Mean firing rate. The mean firing rate during the entire session (15 min) was required to be at least 0.1 spikes/s, corresponding to at least 90 spikes per session.
(2) Trough-to-peak magnitude. We only considered units with a trough-to-peak of at least 50 μV. If the unit was a positive unit[57], we considered peak-to-trough magnitude instead.
(3) Temporal isolation. We quantified temporal isolation using the ISI-index,[26] where ISI1 and ISI2 are the edge values of 2 ms and 20 ms, respectively. Thus, this value was used as a clear refractory period threshold (count in the first 2 ms below 0.2 of the expected count given the counts in the first 20 ms). A threshold of below 0.2 was applied to the ISI index.
(4) Morphological isolation. We quantified waveform isolation using the L-ratio.[27] For that, we used the principal component coefficients calculated by phy, three per channel. A threshold of below 0.05 was used for the L-ratio.

Overall, a total of 2140/2975 units passed all four criteria.

Histology and probe track imaging

Following the termination of experiments, each implanted mouse was anesthetized with isoflurane (induction 3%, 0.5%–0.8% maintenance in 200 mL/min air) and attached to the stereotaxic device. The NP1 probe was carefully removed from the head and cleaned with 2% Targazyme for one hour, followed by rinsing three times with distilled water for reuse. The mouse was removed from the stereotactic device and injected with Ketamine (90 mg/kg) and Xylazine (10 mg/kg) intraperitoneally to prepare for perfusion. The mouse was then perfused with 0.1 M/pH 7.4 phosphate-buffered saline (PBS) and fixed using a 4% paraformaldehyde (PFA, Sigma) solution. The brains were harvested and placed in PFA (4%) for 48 h and sectioned at 50 μm in the coronal plane (VT1200s, Leica). The slices were mounted onto microscope slides with DAPI (F6057, Merck). Images of subject brain slices were acquired to locate probe tracks in an epifluorescence microscope (Ti2 eclipse, Nikon) equipped with a blue filter for DAPI staining and TRITC for DiI marks.

Brain area registration based on histology

Using the software Universal Probe Finder (UPF[56]), each recorded unit was registered with respective brain regions according to the Common Coordinate Framework (CCF; Allen Institute[58]). The histology images were overlaid using the UPF GUI with CCF outlines, and probe tracks were drawn to mark the recorded regions. The UPF outputs included the probe implant location, as well as the depth and the location of every spike cluster. The original UPF code was modified to extract the spike data as well as the camera strobe timestamps using UPF outputs, SpikeGLX outputs (LF and nidq meta files), probe map, KS 2.5, and phy sorted data.

Firing rate by position maps

From this point onwards, all analyses were carried out using custom code written in MATLAB. The "Head_Center" coordinates from DLC, given in pixels, were converted to a position in the arena in cm units. Times during which the mouse moved slower than 1 cm/s were discarded, leaving a median [IQR] of 12.29 [11.67 13.1] min for every session ($N = 20$ sessions). Then, the trajectory and spike positions were binned using a 3×3 cm grid and smoothed using a symmetric 2D Gaussian kernel (SD, 3 cm) to obtain occupancy and spike count maps. A bin-by-bin division of the smoothed spike count matrix by the smoothed occupancy matrix yielded a firing rate map for every unit. The firing rates, which depend on occupancy times, were employed as opposed to the spike counts to enable comparable analyses even when the investigation times of the two stimuli were not time-matched.

For presentation purposes (Figures 4B, 5H, and S4A–S4D, and S5E-H), the rate maps were color-coded from zero (dark blue) to the maximal firing rate of each unit (dark red). In some cases (Figures 4I, 5B, S4E–S4H, and S5A–S5D), the same color code was used for multiple rate maps to better visualize the results. Bins in which the mouse spent less than 1 s were colored white in the figures.

Inter-spike interval shuffling test

We performed an ISI-shuffling test for each unit to compare some of our observations to what may be observed by chance. First, we derived a statistic (e.g., spatial MI, social MI, RMC) from the original spike train. Then, we obtained 5,000 shuffled spike trains from the original spike train of the unit, without changing the behavioral data. In every repetition, we randomly permuted the ISIs of the unit and created a new, ISI-shuffled spike train. We then applied the exact same analysis, deriving a shuffled statistic. We then determined the empirical probability to obtain the original statistic from the distribution of the shuffled statistics.

Asterisks definitions

In all statistical tests throughout this paper, asterisks denote p-value thresholds as follows: *: $p < 0.01$; **: $p < 0.001$; ***:$p < 0.0001$; ns: $p > 0.05$.

Behavioral vs. neuronal preferences in socio-spatial space

The duration of the investigation bouts of each subject with every stimulus was estimated using the TrackRodent software[51]). Corresponding durations were extracted for the pre-encounter epoch, based on the interaction times with the empty stimulus chambers. The procedure yielded four duration values, two for the pre-encounter epoch (next to each empty chamber; T1 and T2 in Figure S2A), and two for the encounter epoch (next to each stimulus chamber; T1' and T2' in Figure S2A). These values across mice and tasks are shown in Figure S2B. These were then used to calculate each unit's behavior contrast index (BCI) as described below. As additional behavioral statistics, we also show the total distance traveled and the number of transitions between stimulus chambers (Figures S2C and S2D).

First, for each epoch separately, we calculated the Kullback-Leibler divergence (D_{KL}) between the distributions of the observed times spent next to each chamber and uniformly distributed durations. Specifically, for the pre-encounter epoch, the observed distribution was: $p = \left[\frac{T_1}{T_1+T_2}, \frac{T_2}{T_1+T_2}\right]$. For the same epoch, the uniform prior was $q = [0.5, 0.5]$. Then, the KL divergence for the pre-encounter epoch, $D_{KL}^{\text{pre-encounter}}$, was calculated using:

$$D_{KL}{}^{pre-encounter} = \sum_{i=1}^{2} p_i \cdot log_2\left(\frac{p_i}{q_i}\right)$$

A corresponding value was estimated for the encounter epoch, namely $D_{KL}^{\text{encounter}}$. The two were then averaged, yielding the D_{KL}^{spatial}, quantifying "how spatially-oriented was the behavior". This estimate quantifies how the investigation durations of the stimulus chambers differed between the pre-encounter and the encounter epochs. For instance, if a specific chamber was investigated for a similar, longer fraction of the investigation durations during the two epochs, it is considered a spatial behavior independent of stimuli in the chambers.

Second, for each chamber separately, we calculated the D_{KL} with respect to a uniform prior for the duration of time spent next to that specific chamber during each epoch, normalized by the total investigation time of that chamber in both epochs. E.g., for chamber 1 the observed distribution was: $p = \left[\frac{T_1}{T_1+T_1'}, \frac{T_1'}{T_1+T_1'}\right]$. For the same epoch, the uniform prior was $q = [0.5, 0.5]$. Using these distributions, we calculated $D_{KL}^{\text{chamber}_1}$. Then, a corresponding $D_{KL}^{\text{chamber}_2}$ value was estimated. These values were then averaged to obtain D_{KL}^{social}, quantifying "how socially-oriented the behavior was". This estimate quantifies how much the exploration durations of each stimulus chamber were modulated during the presence of the social stimuli, averaged for both stimuli. For instance, if both

chambers were uniformly investigated with no stimuli in them (i.e., in the pre-encounter epoch), and one of them was investigated for a longer duration during the social encounter, it is considered a social behavior independent of the specific stimuli position in the experimental arena.

The BCI was defined as the contrast between the above two estimates, namely the difference between spatial D_{KL} and the social D_{KL}, divided by the sum. The BCI ranges from −1 for purely social behavior to 1 for purely spatial behavior. BCI was calculated for each recording session separately, obtaining 20 BCI values, one for every session.

Then, to compare the behavioral preference with a corresponding neuronal metric, we calculated an equivalent index for the spiking activity of every unit, the neuronal contrast index (NCI). For each epoch separately, we counted the number of spikes in proximity to each stimulus chamber. These yielded four spike-count values for the two stimulus chambers and the two epochs (S1, S2, S1', and S2' in Figure S2A). Then, the social and spatial D_{KL} values were calculated as described above for the BCI, measuring D_{KL} between the observed spike count probabilities and a duration-based prior, derived from T1, T2, T1′, and T2'. Specifically, for computing the neuronal $D_{KL}^{spatial}$ during the pre-encounter, we used $p = \left[\frac{S_1}{S_1+S_2}, \frac{S_2}{S_1+S_2}\right]$ as the spike counts probability, and $q = \left[\frac{T_1}{T_1+T_2}, \frac{T_2}{T_1+T_2}\right]$ as the duration-based prior. Similar calculations were done to get the neuronal D_{KL}^{social} for each chamber and for each epoch as described for the BCI. This procedure yielded neuronal $D_{KL}^{spatial}$ and neuronal D_{KL}^{social}, estimating "how spatially-oriented" and "how socially-oriented" the neuronal activity was. The contrast between the neuronal D_{KL}^{social} and $D_{KL}^{spatial}$ values was calculated for every unit, yielding the NCI. This value ranges from −1 to 1, corresponding to purely social to purely spatial neuronal activity.

To quantify the relationship between the BCI and NCI (as shown in Figures 2A–2D), Spearman's rank correlation coefficient (cc) was calculated. Significance was determined using a permutation test.

Last, we assessed the dorsoventral slope of the BCI-NCI cc across PFC subregions (Figure 2E) and bins of distance from the brain surface (Figure 2F). For the latter case, we divided the distances from the brain surface of all 2140 units into 24 equally-populated bins (89 or 90 units per bin). Then, we calculated the mean and SEM of subregion- or bin-specific cc by bootstrapping the data 100 times.[59] Then, we fitted a line to the mean values using the fit.m function of MATLAB, and calculated the slope of this line. To determine if the absolute value of the slope is larger than can be achieved by chance, we randomly permuted the labels (subregion or bin) across units. Repeating the label permutation process 1000 times yielded a distribution of slopes, from which the empirical probability was derived.

Spatial preference analysis

To decide whether a unit had a spatial preference in proximity to one of the stimulus chambers, we calculated for each epoch separately the spatial MI[60] and compared it to shuffled values (ISI shuffling test; 5000 repetitions) to get a *p*-value for spatial modulation. Because MI is non-negative, it is necessarily biased when assessed using a finite sample. The mean of the shuffled MI values was used as an estimate of bias, which was subtracted from the raw estimate.[61] Units with an epoch-specific *p*-value below 0.05/3 (Bonferroni correction for multiple comparisons) and spatial MI above 0.1 bits were considered spatially modulated during that epoch. Then, for the spatially modulated units, a 2D Gaussian was fitted to the rate map of the relevant epoch (using fitgmdist.m, MATLAB), and the fitted Gaussian mean was considered the center of mass of that place field. The spatial preference of the corresponding unit and epoch was then noted according to which stimulus chamber was closer to that center of mass (an example is shown in Figure 3A).

Rate modulation contrast (RMC)

For each unit, we calculated the mean firing rate during every epoch. For each pair of epochs, we calculated the RMC, an index defined as the difference divided by the sum of each pair of mean rates. The RMC values range from −1, if the second rate is much larger than the first, to 1 in the opposite case. A value of 0 indicates that the means are equal. The RMC of every unit during every pair of epochs was compared to 5000 corresponding ISI-shuffled RMCs, yielding an empirical *p*-value. Pairs of epochs with $p < 0.05/3$ (Bonferroni correction for multiple comparisons) and with $|RMC|>0.05$ were considered as exhibiting inter-epoch rate modulation.

For the "rate modulation" criteria (Figures 3F and S6), we used units in which the rate was modulated from the pre-encounter to the encounter epoch, and from the encounter to the post-encounter epoch (according to the criteria above; i.e., the absolute value of each RMC was above 0.05), with an absolute sum of the two RMC values smaller than 0.05.

Classification of units into groups

We looked for modulation patterns associated with the encounter epoch to classify units into groups. Using the above definitions for spatial preference (spatial MI) and inter-epoch rate modulation (RMC analysis), we classified 686 of the 2140 single units into one of four mutually exclusive groups: (1) Units that exhibited spatial modulation during all three epochs (significant spatial MI), a preferred side during the encounter epoch, and preferred the opposite side during the two other epochs, were classified as "social-place-remapping" (e.g., Figures 4A–4G, and S4A–S4D). (2) Units that exhibited spatial modulation only during the encounter epoch, and were not spatially modulated during the two other epochs, were classified as "social-place-coding" (e.g., Figures 4H–4N and S4E–S4H).

(3) ''social-rate-modulation'' units (e.g., Figures 5A–5F and S5A–S5D) were units that were classified to the ''rate modulation'' criteria, and did not exhibit spatial modulation during any epoch. (4) Units that exhibited spatial modulation during all three epochs, and preferred the same side during all epochs, were classified as units with "stable-spatial-preference" (e.g., Figures 5G–5M and S5E–S5H).

For each of the four groups (except for the ''social-rate-modulation'' units), we calculated the probability of units to have a preferred stimulus in a specified task (Figures 4E, 4L, and 5K) using the spatial preference analysis for the encounter epoch only. To test whether the representations of each stimulus given a task were uniform, we used a Chi-squared test with a threshold of $p < 0.05/4$ to correct for the multiple comparisons (4 tasks). A similar analysis compared the probability of the different stimuli being preferred among the different PFC subregions regardless of cell group (Figures 3B–3E).

Brain subregion analysis

For each group of units, we calculated the probabilities of units among the different PFC subregions (Figures 4F, 4M, 5E and 5L). We used Monte Carlo resampling to test whether the probability of observing units classified into a given group is expected by chance. For each of the 2140 single units recorded, we ISI shuffled the spike times (20 iterations) and repeated the entire cell classification process described above. Thus, we obtained the distribution of chance classification of the 2140 units into the four groups (or to none) by chance. We used the mean Monte Carlo-derived prevalence as each group's chance level, and used a normal approximation of the corresponding SD to obtain an empirical p-value (Pmc) indicating the chances to obtain the corresponding prevalence by chance.

To determine whether units are distributed uniformly between PFC subregions, we performed a Chi-squared test, testing the null hypothesis that the prevalence of units in a given group across subregions is uniform. The same approach was used to compare the portions of units for specific subregion analyses: in the PL vs. the IL and the DP vs. the TTd.

Social and spatial information analysis

We performed the following analysis to evaluate and compare the social and spatial contributions to the social representation of space.

For each unit, we computed social and spatial MI values, which were measured in units of bits. For each spike train, spikes from all three epochs of the session were included. Spatial MI was estimated between firing rates and position (binned into 3×3 cm, smoothed by a Gaussian kernel of 3 cm in width, yielding a total of 30 bins on average for every unit). Social MI was estimated between firing rate and a binary variable stating whether there were or were not stimuli in the arena (0 for the pre-encounter, 1 for the encounter, and 0 for the post-encounter). We also estimated the speed MI between the firing rate and the speed of the mouse (based on the magnitude of the first temporal derivative of the mouse's position). For the latter case, we found the speed MI much lower than the other MIs for almost all units and discarded speed from the analysis. Both the spatial and social MIs were de-biased by subtracting from them the mean ISI-shuffled corresponding MIs to allow a fair comparison between them despite their different number of bins (Figures 4G, 4N, 5F, and 5M).

This analysis was also for the feature-based classification of units into ''social'', ''predominantly social'', ''spatial'' and ''predominantly spatial'' as shown in Figure 6. We used this feature-based classification to compute the prevalence of social and spatial units across the different tasks (Figure 6B), subregions of the PFC (Figure 6C), and distance from the brain surface (Figure 6D). To simplify the comparisons, we pooled together the ''social'' and ''predominantly social'' feature dependent units, as well as the ''spatial'' and ''predominantly spatial'' units. The prevalence values were scaled by the total number of units in each pair of groups to obtain comparable measures, which were then compared using Chi-squared tests. Error bars indicate SEM and are estimated using the normal approximation to the binomial error.

The extent of social effect on the population's neuronal activity

The social aspect of spatial representation was observed in all four groups of units. Therefore, we wanted to quantify it on the population level. Thus, two categories were used to estimate the prevalence of social effect in the PFC: ''place remapping'' and ''rate modulation''. Place-remapping was defined in the same manner as in the ''social-place-remapping'' group, i.e., units that modulated their spatial preference only during the encounter epoch compared with the two other epochs. Since rate modulations were observed in all groups, the ''rate-modulation'' category was defined by the RMC analysis (Figure 3F), i.e., this category included units whose firing rate during the encounter epoch was larger or smaller compared with the rates during the two other epochs. A total of 181 ''place remapping'' (Figure S6A, blue and purple) and 225 ''rate modulation'' (Figure S6A, orange and purple) units were used for this analysis. Since 19 units (purple) passed both criteria, this yielded a total of 387 (18% of the recorded PFC units) units with a social effect on the neuronal activity. Although many social effect units were observed in the ESP tasks compared with the other two tasks, the null hypothesis that the distribution of the social units is uniform across tasks was not rejected ($p = 0.07$, Chi-squared test; Figure S6B). The same null hypothesis was rejected across PFC subregions ($p = 0.035$; Figure S6C).

GLM analysis

As an independent procedure, we supplemented the MI analyses by implementing a GLM analysis. We first calculated a single firing rate map for each unit separately for the entire recording duration (pre-encounter, encounter, post-encounter). Second, we fit a 2D

Gaussian model to that rate map using the nlinfit.m function of MATLAB. The model consisted of seven parameters (place field center, width, amplitude, offset, and orientation):

$$G(x,y) = A \cdot \exp\left(- \left[\frac{\left((x - \mu_x)\cos\theta + (y - \mu_y)\sin\theta\right)^2}{2\sigma_x^2} + \frac{\left((y - \mu_y)\cos\theta - (x - \mu_x)\sin\theta\right)^2}{2\sigma_y^2} \right] \right) + Baseline$$

Third, we reconstructed the firing rate from the 2D position (sampled at 30 fps) and the model, denoted as G(x(t), y(t)), which was used for modeling the spatial component of the rate vector. For the social component, we simply used a binary vector (0/1) if there was a social stimulus in the environment. The time vector for all variables was downsampled by taking each 10^{th} sample to avoid time correlations. The logarithm of the actual firing rate vector, R(t), was then fitted, using the glmfit.m of MATLAB, with baseline (a_0), spatial (a_1), social (a_2), and multiplicative interaction (a_3) coefficients:

$$\log(R(t)) \sim a(0) + a(1)\cdot G(x(t),y(t)) + a(2)\cdot S(t) + a(3)\cdot G(x(t),y(t))\cdot S(t)$$

This procedure also yielded *p*-values for each of the four coefficients above, indicating the chance of getting a better fit by chance. We used $p < 0.05/4$ as the threshold for significance for each of the coefficients above. Units were noted as ''GLM Spatial'' if only a_1 was significant and ''GLM Social'' if only a_2 was significant. Units with significant a_3 were denoted as ''GLM Mixed''. The latter case was also subdivided into ''GLM predominantly-social'' if only a_2 and a_3 were significant, and ''GLM predominantly-spatial'' if only a_1 and a_3 were significant.

We found similar and overlapping results with the MI analysis for most units (Table S2B), with some differences related to the different definitions of these analyses. For the main examples presented in Figures 4 and 5, the GLM analysis yielded the expected results. Specifically, the ''social-place-remapping'' unit (Figures 4A–4G) was identified as ''mixed'' (social and spatial); the ''social-place-coding'' unit (Figures 4H–4N) was identified as ''predominantly social''; the ''social-rate-modulation'' unit (Figures 5A–5F) was identified as ''social''; and the ''stable-spatial-preference'' unit (Figures 5G–5M) was identified as ''spatial''.